ASTRONOMY & ASTROPHYSICS
SUPPLEMENT SERIES

Astron. Astrophys. Suppl. Ser. **106,** 39-78 (1994)

A survey of diffuse interstellar bands (3800-8680 Å)*

P. Jenniskens[1] and F.-X. Désert[2,3]

[1] Leiden Observatory, P.O. Box 9513, 2300 RA Leiden, The Netherlands
[2] DEMIRM, Observatoire de Meudon, 92195 Meudon Cedex, France
[3] Institut d'Astrophysique Spatiale, Bat. 121, Université Paris XI, 91405 Orsay Cedex France

Received June 15, 1993; accepted February 8, 1994

Abstract. — A systematic search for diffuse interstellar absorption bands in the spectra of four reddened early type stars has resulted in the detection of 64 new bands and another 69 possible interstellar features. The survey covers the wavelength range from 3800 to 8680 Å, with 0.3 Å resolution, down to a sensitivity limit of about W/E_{B-V}=0.008 Å/mag. The spectra are shown in full length in order to allow a direct comparison with laboratory absorption spectra of candidate diffuse band carriers. Indeed, it is now possible to decide whether stellar or telluric lines mask any diffuse band that is observed in the laboratory, as we show in an example. The example chosen is that of the naphtalene ion, for which we report the detection of two predicted DIBs at 6521 and 6741 Å.

Key words: dust, extinction — stars: individual (HD 30614, HD 21389, HD 190603, HD 183143) — ISM: molecules

1. Introduction

Diffuse interstellar bands (DIBs) are weak absorption features in the near UV, visual, and near infrared spectra of reddened stars that have their origin in the interstellar medium and are typically broader than expected from the Doppler broadening of turbulent gas motions in the interstellar medium. None of the bands have been identified with any certainty, although the first bands were discovered over 50 years ago (Merrill 1934). The location of the bands in the electromagnetic spectrum suggests that these are electronic transitions of relatively small energy difference.

Recent attempts to identify the DIBs have led to a shift of attention from impurities in grains and small gas–phase molecules to the new class of large molecules that are responsible for the mid–infrared emission bands, which are thought to be Polycyclic Aromatic Hydrocarbons (PAH). PAHs are inferred to be present at high abundances in the diffuse medium. Ionized or radical PAH species have transitions in the visual part of the spectrum with considerable oscillator strength (Van der Zwet & Allamandola 1985, Crawford et al. 1985, Léger & d'Hendecourt 1985). Laboratory studies of such ions are hampered by the difficulties met in obtaining accurate position information, but recent studies in inert neon matrices at 4.2 K have proven to be promising (Salama & Allamandola 1992a,b; Ehrenfreund et al. 1992).

A need has grown for a systematic survey of diffuse interstellar bands, with modern detectors, and a comprehensive presentation that can be used for comparison with laboratory results (see the similar suggestions by Herbig & Leka 1991). This paper reports on such a survey, with no intention to emphasise or to speculate on one of many suggested DIB carriers. A discussion of the statistical aspects of the survey will be published elsewhere.

The main characteristics of the survey are a high spectral resolution ($\Delta\lambda$ = 0.3Å) over a wide spectral range (3800–8680 Å), but consequently considers only a small sample of reddened stars. Four reddened stars were chosen such that they cover a range in reddening, spectral type, and relative radial velocity between star and interstellar dust. These features allow a near certain assignment of absorptions to either diffuse bands, stellar photospheric lines, atmosphere lines, or detector irregularities. We show the spectra at full length, so that one can check if a position from a laboratory spectrum is masked by stellar or atmospheric lines.

This paper pays tribute to the first and only systematic survey published until now, that by Herbig (1975), obtained from spectra recorded on photographic plates over the region 4400–6850 Å ($\Delta\lambda \sim 0.7$Å). Some 39 DIBs were recorded with certainty. The introduction of solid state de-

Send offprint requests to: P. Jenniskens, NASA/Ames Research Center, Mail Stop 239-4, Moffett Field, CA94035-1000, U.S.A.

*From observations obtained at Observatoire de Haute-Provence, France

tectors has since led occasionally to the discovery of new diffuse bands. Sanner, Snell & Vanden Bout (1978) published a low resolution survey of the 6500–8900 Å region, using a Reticon detector ($\Delta\lambda = 0.94$ Å), adding 3 certain DIBs and two possible ones. Recently, Herbig (1988) published a deep survey (down to 2 mÅ in equivalent width for a 1 Å DIB) of a window between 6770 and 6862 Å at a resolution of 0.7 Å . These data show a crowding of diffuse bands, almost to the point of saturation. This held the promise that many more DIBs could be discovered in a more extended search, which lead us to attempt this survey. After we started in Sept. 1990, Herbig & Leka (1991) published from similar CCD observations a second set of 20 new diffuse bands from a few windows in the red, bringing the total number of diffuse interstellar bands to about 96. Throughout the paper, we adopt Herbig's notation by indicating each DIB by the central wavelength position at which it is found, e.g. λ5780. And, following the usual convention, we refer to wavelengths in air and wavenumbers in vacuum.

This paper is ordered as follows. Sections 2 and 3 deal with the selection of program stars, the instrumental characteristics, and the parameters derived from the spectra. In Sect. 4 (Table 3) a catalogue of diffuse bands is presented. A set of plots that show the spectra at full length are given in the Appendix. In Sect. 5 we give an example of how the survey can be used in comparing observations with laboratory data, keeping in mind the limitations of the survey which are discussed in Sect. 6.

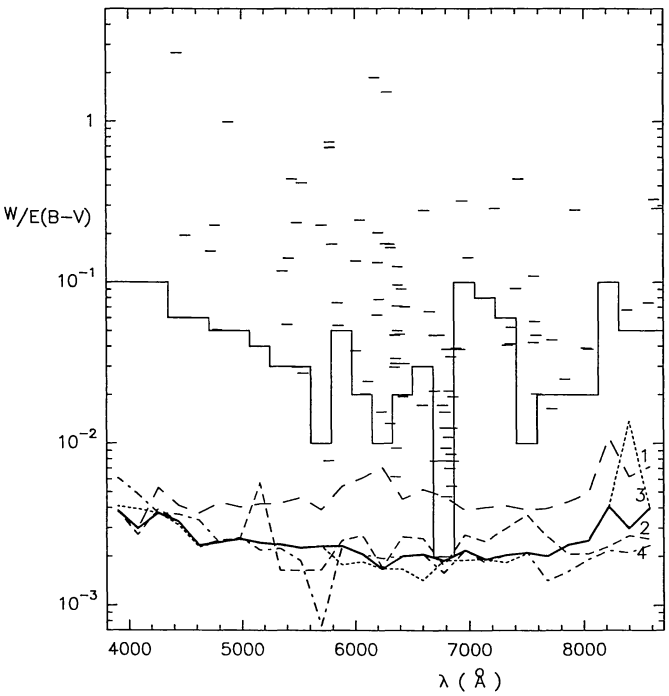

Fig. 1. Dashed lines show the sensitivity limit (1 σ) for a typical 1 Å FWHM diffuse interstellar band due to photon and readout noise for each of the four reddened stars. An estimate of the 1 σ detection limit for DIBs in this survey is given by a bold line. The sensitivity limit is compared to those of previous surveys (continuous thin line at $\simeq$3 σ) and previously known DIBs

2. The observations

2.1. *The instrument*

The Aurelie spectrograph (Gillet 1990) has the advantageous property of enabling a quick change of the central wavelength by a software command. It serves the 1.52 m Coude telescope of the *Observatoire de Haute Provence*, France. The detector consists of a 2048 diode linear Reticon array, which is read by a Thomson TH7832 CCD system of two alternatingly reading CCDs with 750×13 μm pixel size. Each spectrum covers 200 Å.

The total wavelength range (3800–8680 Å) is covered by 27 windows. The central wavelength of each window is shifted by 180 Å from the previous one, starting at a central wavelength of 3900 Å . The overlap of 20 Å is chosen because the first and last pixels of the detector show strong pixel to pixel sensitivity variations and the wavelength calibration is more uncertain here.

More precisely, the spectral range per window is 200 Å in the red and 210 Å in the blue. Two gratings were used. Both have 1.2 10^4 lines cm^{-1}. Below 7500 Å , grating No. 2 (blaze angle at 5000 Å) gave a resolution of $\Delta\lambda = 0.300$ Å . Between 6000 Å and 7500 Å , this grating is used in combination with a filter OG 515(3) in order to avoid second order image overlap. Above 7500 Å, grating No. 5 is used in first order in combination with filter OG 590(3), which results in a slightly better resolution: $\Delta\lambda = 0.275$ Å. Each resolution element is fully sampled by projection on three pixels of the CCD, i.e. 0.1 Å /px.

The total wavelength coverage is limited by the sensitivity of the system, which varies with wavelength. The grating efficiency is nearly constant over the wavelength range considered, but the detector efficiency peaks at 6500 Å (η = 0.72) and falls off to η = 0.4 at 3700 Å and 8600 Å (Gillet 1990). The system can handle infrared emission up to 10400 Å, but the decreasing detector sensitivity conspires with the decreasing brightness of the black body continuum of the program stars and therefore one needs long integration times. The sensitivity at short wavelengths is limited by the increase of continuum extinction of interstellar dust and by the optical transparency of the glass fibres used in the spectrograph, which falls off quickly below 3700 Å.

2.2. *The selection of program stars*

The program stars have been selected in order to fullfil a number of conflicting constraints: allow an easy detection of DIBs, allow a certain discrimination against other sources of absorption and, with less weight, have a repre-

Table 1. Physical parameters of the program stars and the interstellar matter in the lines of sight. [1] Data from Aiello et al. (1988). [2] $A_{c\ 4430}$ from Snow, York and Welty (1977). [3] Data from this study. [4] Extinction curve parameters (Jenniskens and Greenberg 1993) in the scheme of Fitzpatrick and Massa (1988) of curves by Aiello et al. (1988). The extinction data for HD21389 are derived from A.N.S. data (Wu et al. 1981). [5] Stellar and interstellar absorptions, radial heliocentric velocities and line widths from our data. Radial velocity (v) in km s^{-1}. [6] Linewidth and relative position, in Å, for a wavelength of 5000 Å

HD	30614 αCam	21389	190603	183143	34085 βOri	120315 ηUMa
α_{1950}	04h49m	03h26m	20h03m	19h25m	05h15m	13h46m
δ_{1950}	+66°16'	+58°42'	+32°05'	+18°12'	-08°12'	+49°34'
Int. time (s)	>500	>800	>600	>500	>10	>60
purpose	redd.	redd.	redd.	redd.	*line	atmos.
location	embedded	background	embedded	background	-.-	-.-
E_{B-V} [1]	0.30	0.54	0.72	1.28	0.00	0.01
V (mag)[1]	4.29	4.54	5.64	6.87	0.12	1.86
SpT [1]	O9.5Ia	AOIae	B1.5Ia	B7Ia	B8Iae:	B3V
Ac_{4430} [2]	3.3	7.5	8.2	15.0	0.0	0.0
W_{5780} [3]	0.113	0.362	0.326	0.718	0.00	0.00
W_{6284}/E_{B-V}	1.37	2.15	1.55	1.68	0.00	0.00
W_{5797}/W_{5780}	0.30	0.19	0.25	0.25	-.-	-.-
W_{6177}/W_{6284}	0.59	0.39	0.34	0.54	-.-	-.-
c_2 [4]	0.91	(0.66)	0.88	0.30	-.-	-.-
$\pi c_3/2\gamma$	5.36	(7.99)	4.88	6.13	-.-	-.-
γ	0.94	(1.09)	0.92	0.93	-.-	-.-
x_o	4.56	(4.61)	4.63	4.61	-.-	-.-
c_4	0.14	-.-	0.04	0.41	-.-	-.-
R_V	3.01	$\sim$ 3.5	3.04	2.91	-.-	-.-
v_{ism} [5](km/s)	-5(2)	-12(3)	-10(2)	-3(3)	-.-	-.-
v_* (km/s)	+19(4)	-6(3)	+21(5)	+15(2)	+20(3)	-11
$v.\ \sin i_*$ (km/s)	174(15)	41(5)	63(7)	60(6)	58(7)	205
FWHM$_*$ [6] (Å)	2.9(0.3)	0.68(0.06)	1.1(0.1)	1.0(0.1)	1.0(0.1)	3.4
FWHM$_{ism}$ (Å)	0.46	0.45	0.61	0.76	-.-	-.-
$\Delta\lambda_{ism-*}$ (Å)	+0.4	+0.1	+0.5	+0.2	-.-	-.-

sentative DIB spectrum for average diffuse medium conditions.

The means of optimalising the detectability of DIBs in the spectra are the following. A number of stars are chosen which have a variable amount of matter in front of the star but are of widely varying stellar type. This results in a gradual increase of DIBs along the series of stars, while stellar lines vary irregularly. We chose a high spectral resolution in order to have high contrast between the DIBs and the continuum, to be able to see the relative Doppler motion of star and interstellar gas, and to obtain good atmosphere line subtraction, but consequently we were able to observe only a small number of reddened early–type stars.

Few stars have both strong brightness V and strong reddening E_{B-V} to allow relatively short integration times. Some relevant parameters of the chosen program stars are listed in Table 1. After a try–out on star HD 30614, we observed the stars HD 21389, HD 190603, and HD 183143 at three times higher signal to noise, down to a sensitivity limit of 0.002 Å /mag in W/E_{B-V} (1σ) for a typical DIB of FWHM = 1 Å (Fig. 1). This allowes the detection of all of the DIBs in Herbig (1988), although the weakest are only marginally detected. Integration times vary from 10 to 60 minutes per spectrum.

We found the DIBs in these lines of sight to have band strengths close to the diffuse medium average, $W_{6284}/E_{B-V} \sim 2.0$, whereas in dense clouds this ratio drops below 1.0 (Jenniskens et al. 1993). Also the diffuse band ratio's of λ5797 versus λ5780 and of λ6177 versus λ6284 are characteristic for the diffuse medium (0.25, 0.55 respectively). However, both the band intensity with respect to E_{B-V} and the relative band intensities show significant differences between the four lines of sight. Notably, the embedded objects HD 30614 (a runaway star) and HD 190603 have slightly weaker DIBs per unit reddening than HD 21389 and HD 183143. As a result, for example, HD 190603 is found to have slightly weaker DIBs relative to HD 21389 in part of the spectrum.

Telluric lines, originating in the Earth's atmosphere, were detected in the spectrum of the fast rotating B3V star HD 120315. Occasionally, we have used as such ref-

erence stars HD 32630 (in combination with HD 21389) and HD 177724 (in combination with HD 190603 and HD 183143). Spurious absorptions due to remnants of the detector pixel to pixel sensitivity variations can be discriminated against by allowing for small (random) variations in the central wavelength of a window (typically a few Å from star to star) and by recognizing that the detector ensemble was changed three times between the epochs of observation, as a result of which not all spectra in a window show the same flatfielding remnants (Fig. 2). Finally, in order to help recognizing DIBs among stellar lines, we have observed the bright non–reddened star HD 34085, which has a similar spectral type as the most reddened star HD 183143 (as well as HD 21389).

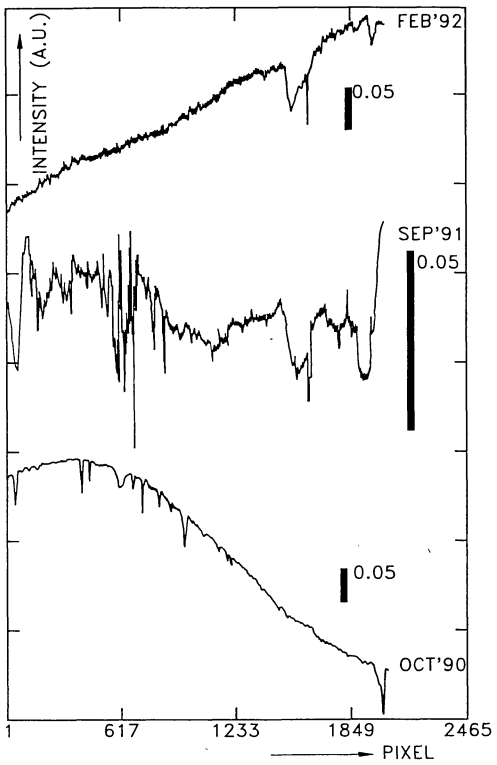

Fig. 2. Examples of flatfielding curves, which show the detector pixel–to–pixel sensitivity variation in several epochs of observation

3. Reduction of the observations

3.1. *The spectra*

The observed spectra are corrected for detector offset and pixel to pixel sensitivity variations (flat fielding), the latter by means of five exposures of twice the star signal with a Tungsten calibration lamp. The dark current was found negligible. The spectra are normalised to unity by fitting a first or second order polynomical to an adopted continuum. This limits the broadness of detectable DIBs to a FWHM ~50 Å. Narrow features in emission were identified as cosmic rays and subsequently removed. This may have included an occasional atmospheric emission line. On average 1 cosmic ray was found per spectrum of 10–30 minutes integration time. The wavelength scale was calibrated with a Thorium–Argon emission lamp, which produced 10–30 lines per window, using the published wavelengths by D'Odorico et al. (1984). Where needed, the telluric lines were removed from the spectra (Herbig 1975, Benvenuti & Porceddu 1989):

$$I_{\rm corr} = I \; / \; I_{\rm ref}^{\alpha} \qquad (1)$$

where $\alpha = \tau/\tau_{\rm ref}$ is the atmospheric line optical depth ratio which was determined iteratively. Reduction was done at O.H.P. and at the *Institut d'Astrophysique de Paris* using the IHAP package (Middleburg 1981). The actual measurements on the spectra and plots have been done with the IDL package.

The spectra were obtained in four observing runs, in about 16 nights of observation: on 7–10 Sept. 1990, 21–24 Sept. 1991, 11–17 Febr. 1992, and 8–10 July 1992. Each time the Earth's velocity adds a different component to the observed radial velocity of the lines. The spectra were corrected to a common heliocentric velocity. And the Doppler motion of the interstellar matter was taken into account by shifting all spectra to a laboratory rest wavelength system. The Doppler shift needed ($\Delta\lambda/\lambda$) was derived from the position of the known interstellar atomic or molecular lines of CaII, NaD, KI and the system CH and CH^+ (Table 1 and Table 2).

Table 2. The interstellar lines of atoms and small molecules. Average values are derived according to values in the DIB catalogue. $\lambda_{\rm rest}$ and $\lambda_{\rm c}$ are the laboratory wavelength (in air) and our measurement respectively after correction for heliocentric and interstellar velocities. The FWHM (FW) is not corrected for optical depth effects, which are considerable for CaII, NaI, and KI. σ refers to the 1 sigma scatter in individual measurements

Ident.	$\lambda_{\rm rest}$	$\lambda_{\rm c}$	σ	FW	σ	$\frac{W_\lambda}{W_{5780}}$	σ
Ca II	3933.664	3933.75	0.05	0.73	0.33	0.810	0.176
CH^+	3957.700	3957.67	-.-	0.44	-.-	0.025	-.—
Ca II	3968.47	3968.41	0.06	0.62	0.16	0.345	0.045
Ca I	4226.73	4226.88	0.22	0.38	0.12	0.009	0.003
CH^+	4232.539	4232.72	-.-	0.61	-.-	0.059	-.—
CH	4300.321	4300.34	-.-	0.45	-.-	0.014	-.—
Na I	5889.953	5889.95	0.02	0.65	0.03	0.837	0.287
Na I	5895.923	5895.92	0.03	0.63	0.02	0.815	0.299
K I	7664.907	7664.94	0.07	0.70	0.04	0.334	0.071
K I	7698.979	7698.99	0.12	0.66	0.06	0.183	0.038

3.2. *The DIB parameters*

A list is compiled of certain (+), probable (o) and possible (doubtful, –) diffuse interstellar bands (Table 3). Diffuse bands are features that align in wavelength, show

an increase with reddening and are not found in the non–reddened star and the telluric absorption spectrum. Doubtful are cases which violate one of these criteria, e.g. due to contamination by stellar lines or due to noise in the data.

For each DIB three parameters are listed in the DIB catalogue (Table 3):

1. The equivalent width (W, in Å) is proportional to the column density of the DIB carriers, because all absorptions are optically thin, and, in case of sets of related DIBs, W reflects the relative oscillator strength.

2. The central wavelength (λ_c in Å) is the laboratory rest wavelength in air.

3. The full width at half maximum (FWHM, in Å) reflects the broadness of the feature.

The equivalent width is measured interactively by putting the cursor at the estimated continuum level, on each side of the feature, and calculating:

$$W = \Sigma_i (1 - \frac{I_i}{I_i^0}) \Delta\lambda, \qquad (2)$$

where I^0 is the continuum baseline and I is the observed intensity and the sum runs over the pixel indices in the feature ($\Delta\lambda$ is the pixel width). In the case of shallow features mixed with stellar lines, the equivalent width of the latter is determined separately and subtracted.

The FWHM of each DIB, and of each component, is calculated from this equivalent width and from the depth of the feature (A_c) with:

$$\mathrm{FWHM} = W/(1.0645 * A_c) \qquad (3)$$

This is an exact formula if the feature has a gaussian profile (although we did not try any gaussian fitting here). The values of equivalent width and FWHM are in relatively good agreement with Herbig (1975, 1988) and Herbig & Leka (1991), although there is a systematic difference in the sense that our values are typically 20% smaller (Fig. 3).

For shallow DIBs with FWHM larger than 5 Å and in the case of complex structures, the depth was estimated interactively. For more narrow features, the depth was taken to be $\min(I/I^0)$. This causes an underestimation of the FWHM of weak DIBs, because noise adds to the central depth. We corrected for this by adding $\Delta A_c = 0.0020$ for HD 30614 and $\Delta A_c = 0.0008$ for the other reddened stars, which results in a similar average FWHM for all stars. Note that the FWHM is *not* corrected for Doppler broadening and instrumental broadening.

The position of the centroid of the profile was measured as a weighted mean over the whole band:

$$\lambda_c = \Sigma_i \lambda_i (1 - \frac{I_i}{I_i^0}) \Delta\lambda / W, \qquad (4)$$

For obvious cases of non–gaussian DIBs, usually a decomposition into two gaussian components was made following Herbig (1975). For shallow DIBs, the central wavelength was estimated by eye. Column 4 in Table 3 contains wavenumbers in vacuum, where $\nu_c = 0.999724/\lambda_c$ (cm^{-1}).

The tabulated values are averaged values of the three reddened stars HD 21389, HD 190603 and HD183143, which usually have the largest signal–to–noise ratio. No significant profile variations are found. The three stars are given equal weight.

Because there do exist significant variations of W/E_{B-V} towards our program stars, the average value listed in the final columns of Table 3 has been derived as follows. The three values of W for HD 21389, HD 190603, and HD 183143 are normalised to λ5780 and subsequently averaged. This mean is then normalised to $E_{B-V} = 1$ using the ratio $W_{5780}/E_{B-V} = 0.561$ of HD 183143. As a result, the values listed in the final two columns of Table 3 *should be characteristic for diffuse medium material per unit amount of reddening.*

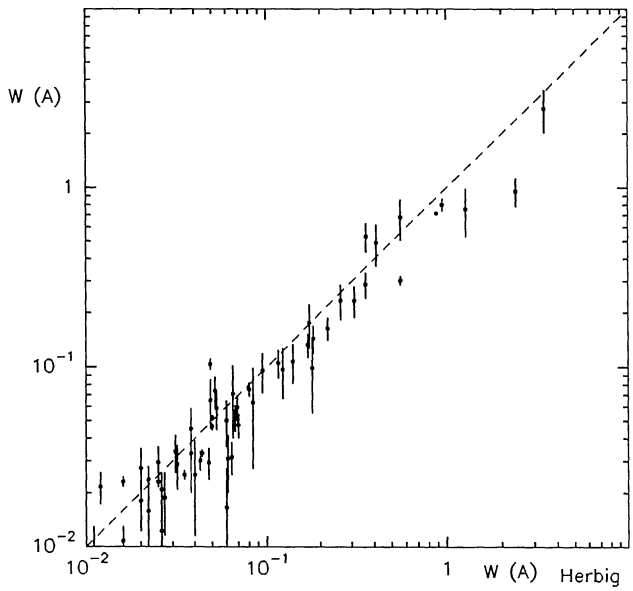

Fig. 3. Comparison of equivalent widths from this work (y axis) and data from Herbig (1975, 1988) and Herbig & Leka (1991). Our data tend to lie 20% below the dotted one–to–one correspondence line. We have excluded from this plot the bands which are decomposed into several components

3.3. *Known DIBs that were not initially detected*

We checked, *a posteriori*, if all known DIBs from previous publications had been detected. Table 4 gives the cases where we missed some previously reported DIBs and the possible reason. Most of these are merely too weak to be detected with certainty. Only a few DIBs are missed as a result of the small number of stars in our sample, most of these due to stellar line contamination. Only one relatively strong DIB was missed (λ6367.31) and included in

Table 3. A catalogue of diffuse interstellar bands. It contains certain (+), probable (o), and uncertain or questionable (-) idendifications from the DIB survey alone, except for the 5780 and 6284 Å windows which were extensively covered by Jenniskens & Désert (1993) and Désert et al. (1994). For each band, one can find the average value of the centroid position in Å in a laboratory rest frame, the full width at half maximum (in Å), the individual equivalent width for the four observed lines–of–sight and an average value of the equivalent width normalised to $E_{B-V} = 1$. Undefined values are noted -1.00. References are BB37: Beals & Blanchet 1937, C85: Chlewicki 1985, C87: Chlewicki et al. 1987, F83: Ferlet et al. 1983, FD84: Ferlet & Dennefeld 1984, G76: Geary 1976, Ga84: Gammelgaard 1984, HaS81: Hayden–Smith et al. 1981, Heg22: Heger 1922, H67: Herbig 1967, H75: Herbig 1975, H88: Herbig 1988, HL91: Herbig & Leka 1991, HS82: Herbig & Soderblom 1982, Ho84: Hobbs 1984, JD93: Jenniskens & Désert 1993, M34: Merrill 1934, M91: Morell et al. 1991, S78: Sanner et al. 1978, T90: Torres–Dodgen 1990, W58: Wilson 1958

cert	L	err	Nu(cm-1)	FWHM	err	HD30614	21389	190603	183143	W/EB-V	err	cross-reference
o	4176.47	3.25	23936.9	23.33	2.15	0.106	0.209	0.343	0.417	0.427	0.158	-
-	4427.57	1.23	22579.4	0.34	0.07	0.002	0.004	0.006	0.011	0.009	0.002	-
+	4428.88	1.35	22572.7	12.33	2.06	0.576	1.113	1.636	2.488	2.231	0.595	BB37
+	4501.80	0.70	22207.2	2.51	0.10	-1.00	-1.00	-1.00	0.250	0.195	0.020	H66, M91
-	4595.00	3.00	21756.7	28.00	5.00	-1.00	0.200	-1.00	0.680	0.451	0.160	-
-	4665.47	1.37	21428.1	4.07	1.02	-1.00	0.078	0.139	0.152	0.165	0.071	-
+	4726.59	0.07	21151.0	1.25	0.17	0.008	0.012	0.025	0.054	0.036	0.014	H75
+	4727.06	0.17	21148.9	3.92	0.49	0.021	0.039	0.060	0.114	0.087	0.023	(H75)
+	4761.67	0.58	20995.2	25.33	1.19	0.182	0.310	0.381	0.865	0.623	0.111	H67, H75
+	4762.57	0.32	20991.2	2.10	0.32	0.019	0.050	0.051	0.084	0.079	0.011	H75
+	4780.09	0.29	20914.3	1.45	0.31	0.005	0.024	0.048	0.059	0.057	0.025	H67, H75
+	4824.00	2.00	20723.9	32.47	2.90	0.101	0.214	0.301	0.594	0.452	0.099	-
+	4880.35	0.27	20484.6	1.35	0.30	0.003	0.007	0.019	0.027	0.022	0.011	-
+	4881.83	0.65	20478.4	19.67	2.38	0.125	0.256	0.433	0.810	0.611	0.184	W58
+	4963.96	0.04	20139.6	0.63	0.16	0.002	0.005	0.012	0.022	0.016	0.007	-
o	4969.67	1.53	20116.4	33.70	1.85	0.288	0.264	0.406	0.446	0.501	0.193	-
o	4984.73	0.12	20055.7	0.65	0.17	0.002	0.017	0.004	0.011	0.014	0.011	-
-	5039.10	1.13	19839.3	17.87	3.04	0.076	0.122	0.197	0.380	0.284	0.080	-
+	5109.70	2.40	19565.2	11.78	6.40	0.054	-1.00	0.182	0.278	0.274	0.070	-
+	5362.14	0.90	18644.1	5.95	0.69	0.023	-1.00	0.054	0.084	0.082	0.020	H67, H75
+	5363.60	0.14	18639.0	1.99	0.04	0.003	-1.00	0.013	0.050	0.032	0.012	-
+	5404.56	0.26	18497.7	1.25	0.13	0.007	0.025	0.018	0.053	0.038	0.006	H75
+	5418.40	0.66	18450.5	8.07	0.72	0.042	0.035	0.068	0.078	0.080	0.036	H67, H75
+	5449.63	0.12	18344.8	13.40	1.64	0.052	0.149	0.146	0.290	0.244	0.014	H67, H75
o	5456.00	0.00	18323.3	27.05	2.47	0.073	-1.00	0.101	0.110	0.134	0.064	-
+	5487.43	0.43	18218.4	5.36	2.16	0.040	0.083	0.075	0.119	0.121	0.021	H75
+	5487.49	0.16	18218.2	1.79	0.83	0.014	0.027	0.049	0.095	0.069	0.023	-
+	5494.14	0.14	18196.1	0.65	0.07	0.005	0.024	0.010	0.029	0.027	0.011	H75
+	5508.35	0.03	18149.2	3.54	0.32	0.050	-1.00	0.083	0.144	0.132	0.022	(H75)
o	5524.89	0.21	18094.9	3.73	0.95	0.015	0.041	0.024	0.067	0.054	0.011	-
+	5535.68	0.28	18059.6	12.92	14.51	0.021	0.034	0.044	0.108	0.073	0.017	-
+	5537.00	1.73	18055.3	22.57	1.07	0.078	0.157	0.208	0.292	0.285	0.073	H75
-	5540.98	1.10	18042.3	1.56	0.04	0.004	-1.00	0.007	0.022	0.015	0.004	-
+	5544.97	0.05	18029.3	0.79	0.08	0.008	-1.00	0.012	0.024	0.020	0.001	H75
+	5609.96	0.23	17820.5	1.74	0.35	0.004	0.017	0.021	0.052	0.035	0.008	-
+	5704.75	0.39	17524.4	6.64	0.63	0.034	0.053	0.049	0.087	0.081	0.009	-
+	5705.13	0.11	17523.2	2.15	0.24	0.014	0.064	0.053	0.115	0.096	0.005	H67
+	5719.43	0.10	17479.4	0.93	0.09	0.008	0.007	0.007	0.017	0.012	0.001	-
+	5747.81	0.08	17393.1	2.32	0.25	0.029	0.028	-1.00	0.053	0.044	0.001	-
o	5762.50	0.33	17348.8	0.66	0.23	-1.00	0.003	0.004	0.014	0.008	0.003	JD93
+	5766.25	0.14	17337.5	0.92	0.20	0.002	0.006	-1.00	0.021	0.013	0.005	C87
o	5769.10	0.20	17328.9	0.8	0.20	-1.00	-1.00	-1.00	0.004	0.003	0.002	JD93
+	5772.60	0.04	17318.4	1.03	0.41	0.004	0.008	-1.00	0.033	0.020	0.010	JD93
+	5776.08	0.23	17308.0	0.85	0.22	0.001	0.005	0.004	0.017	0.010	0.004	JD93
+	5779.48	0.26	17297.8	15.50	1.73	0.143	0.442	0.354	0.752	0.647	0.053	Heg22, M34
+	5780.59	0.05	17294.5	2.07	0.16	0.113	0.362	0.326	0.718	0.579		Heg22, M34
o	5784.90	0.25	17281.6	1.0	0.30	-1.00	-1.00	-1.00	0.023	0.018	0.006	JD93
+	5789.06	0.54	17269.2	1.13	0.33	0.005	0.007	0.009	0.011	0.012	0.004	JD93
+	5795.23	0.32	17250.8	4.09	0.67	0.021	0.067	0.063	0.162	0.117	0.012	H67, H75
+	5797.11	0.05	17245.2	0.97	0.08	0.034	0.069	0.080	0.178	0.132	0.019	Heg22, M34, H75
+	5809.12	0.06	17209.5	1.10	0.25	-1.00	0.009	0.012	0.016	0.016	0.004	-
+	5809.96	0.09	17207.0	2.55	0.45	-1.00	0.021	0.027	0.038	0.037	0.009	JD93
o	5814.50	0.30	17193.6	0.40	0.20	-1.00	-1.00	0.001	0.008	0.004	0.003	JD93
o	5818.85	0.30	17180.8	0.49	0.17	-1.00	0.003	0.003	0.003	0.004	0.002	JD93
o	5828.40	0.20	17152.6	0.31	0.10	-1.00	0.001	0.001	0.005	0.003	0.001	JD93
+	5844.19	0.22	17106.3	3.04	0.63	0.045	0.054	0.031	0.112	0.077	0.019	H67, H75
+	5849.78	0.09	17089.9	1.03	0.04	0.019	0.025	0.027	0.069	0.048	0.008	H67
o	5853.95	0.82	17077.7	1.79	0.41	0.002	0.002	0.021	0.025	0.020	0.017	-
-	5982.00	0.32	16712.2	1.01	0.05	0.003	0.010	0.008	0.018	0.015	0.001	-
+	6004.55	0.55	16649.4	1.19	0.37	0.018	0.014	0.011	0.036	0.024	0.005	HL91
+	6010.58	0.11	16632.7	3.46	0.25	0.032	0.070	0.104	0.158	0.141	0.038	H75
+	6019.34	0.10	16608.5	0.90	0.16	0.007	0.008	0.017	0.014	0.018	0.011	-
+	6027.39	0.20	16586.3	1.61	0.75	0.013	0.014	0.023	0.030	0.029	0.010	-
+	6037.56	0.23	16558.4	1.84	0.28	0.016	0.021	0.026	0.048	0.039	0.006	-
+	6045.27	0.87	16537.3	14.23	3.36	0.052	0.134	0.116	0.182	0.189	0.037	H75
o	6060.41	0.67	16496.0	1.20	0.33	0.008	0.010	0.009	0.030	0.019	0.005	-
+	6065.38	0.04	16482.4	0.94	0.13	0.004	0.010	0.006	0.018	0.014	0.003	-
o	6070.53	1.20	16468.5	0.81	0.14	0.000	0.005	0.003	0.022	0.010	0.007	-
+	6089.80	0.08	16416.4	0.82	0.15	0.008	0.011	0.007	0.025	0.017	0.004	HL91
o	6108.21	0.19	16366.9	0.58	0.09	0.002	0.004	0.003	0.011	0.007	0.002	-
+	6113.22	0.17	16353.5	1.03	0.16	0.013	0.016	0.012	0.042	0.027	0.006	H75
o	6116.65	0.08	16344.3	0.52	0.20	0.002	0.006	0.002	0.011	0.007	0.003	-
+	6139.77	0.03	16282.7	0.88	0.19	0.011	0.006	0.007	0.025	0.014	0.005	-
+	6177.27	0.67	16183.9	23.00	3.68	0.242	0.450	0.376	1.155	0.773	0.140	W58
o	6189.53	0.52	16151.8	0.86	0.01	-1.00	0.006	0.009	0.007	0.010	0.005	-
+	6194.87	0.34	16137.9	0.59	0.27	-1.00	0.002	0.003	0.012	0.006	0.003	HaS81
+	6196.19	0.33	16134.5	0.65	0.07	0.015	0.037	0.032	0.083	0.061	0.005	H67
o	6199.21	0.59	16126.6	0.77	0.20	0.003	0.007	0.003	0.008	0.008	0.003	-
+	6203.19	0.38	16116.3	1.21	0.05	0.021	0.057	0.069	0.134	0.107	0.016	H67, H75
+	6204.33	0.30	16113.3	3.93	0.05	0.062	0.095	0.132	0.223	0.189	0.042	H67, H75
+	6207.83	1.01	16104.2	11.70	3.01	0.035	0.090	0.078	0.154	0.136	0.010	-
+	6212.19	0.40	16092.9	1.23	0.13	0.006	0.009	0.006	0.022	0.014	0.004	C85
o	6215.71	0.52	16083.8	1.06	0.55	0.005	0.005	0.002	0.012	0.007	0.003	-
o	6223.65	0.43	16063.3	0.54	0.19	-1.00	0.003	0.002	0.010	0.005	0.002	-
+	6234.27	0.36	16035.9	0.83	0.08	0.007	0.014	0.016	0.019	0.022	0.007	C85, (H75)
o	6236.58	0.81	16030.0	0.57	0.13	0.004	0.003	0.005	0.008	0.007	0.002	JD93
+	6270.06	0.33	15944.4	1.03	0.15	0.017	0.047	0.032	0.118	0.076	0.019	H67, H75
+	6270.36	0.35	15943.6	3.56	0.25	0.036	0.048	0.025	0.076	0.061	0.016	H75
+	6278.29	0.73	15923.5	0.64	0.18	0.011	0.010	0.007	0.019	0.015	0.002	JD93
o	6280.52	0.38	15917.8	0.83	0.14	-1.00	0.012	0.018	0.015	0.021	0.010	JD93
+	6281.07	0.45	15916.4	8.47	0.50	0.370	0.774	0.739	1.440	1.237	0.076	JD93
+	6284.31	0.33	15908.2	2.58	0.07	0.040	0.385	0.376	0.707	0.618	0.049	M34
o	6287.12	0.41	15901.1	0.62	0.27	0.009	0.016	0.004	0.012	0.014	0.010	JD93
o	6289.60	0.81	15894.9	1.08	0.20	0.005	0.009	-1.00	0.012	0.012	0.003	JD93
+	6308.93	0.25	15846.2	2.37	0.41	-1.00	0.036	0.033	0.070	0.058	0.001	HL91
+	6315.00	2.11	15830.9	21.23	1.50	0.133	0.173	0.262	0.389	0.352	0.100	H75
+	6317.58	0.20	15824.5	2.06	0.16	0.016	0.046	0.038	0.041	0.058	0.022	JD93
o	6321.53	0.44	15814.6	1.45	0.52	-1.00	0.007	0.010	0.022	0.016	0.004	-
+	6325.10	0.25	15805.6	0.83	0.16	-1.00	0.005	0.015	0.023	0.018	0.009	JD93
+	6330.42	0.19	15792.4	1.02	0.11	0.010	0.011	0.010	0.022	0.018	0.000	JD93

Table 3. continued

cert	L	err	Nu(cm-1)	FWHM	err	HD30614	21389	190603	183143	W/EB-V	err	cross-reference
+ 6353.49	0.24	15735.0	1.83	0.17	0.011	0.015	0.024	0.053	0.036	0.011	H75
+ 6359.53	1.27	15720.1	37.33	11.51	0.077	0.240	0.346	0.756	0.536	0.132	HL91
+ 6362.35	0.04	15713.1	1.34	0.22	0.006	0.016	0.012	0.033	0.025	0.003	HL91 (H75)
+ 6367.22	0.07	15701.1	0.88	0.21	0.005	0.012	0.011	0.016	0.017	0.004	Ho84
+ 6376.07	0.03	15679.3	0.74	0.11	0.006	0.018	0.011	0.035	0.026	0.005	H75
+ 6377.87	0.12	15674.9	3.48	1.42	0.008	0.014	0.022	0.041	0.032	0.008	-
+ 6379.27	0.08	15671.4	0.79	0.05	0.026	0.038	-1.00	0.118	0.078	0.024	H75
- 6383.04	0.35	15662.2	0.96	0.20	0.003	0.018	0.008	0.027	0.022	0.007	-
+ 6397.39	0.27	15627.0	1.37	0.40	0.003	0.013	0.011	0.043	0.025	0.008	HL91
+ 6413.50	0.26	15587.8	8.07	1.55	0.024	0.064	0.041	0.100	0.085	0.015	HL91
o 6413.90	0.29	15586.8	0.88	0.12	0.006	0.014	0.007	0.015	0.016	0.006	HL91
+ 6425.72	0.20	15558.2	0.71	0.06	0.008	0.011	0.011	0.023	0.019	0.001	H67, H75
+ 6439.34	0.24	15525.2	1.02	0.30	0.010	0.005	0.014	0.035	0.020	0.011	HL91
+ 6445.53	0.36	15510.3	1.17	0.38	0.007	0.043	0.012	0.067	0.048	0.006	HL91
+ 6449.13	0.27	15501.7	1.15	0.20	0.009	0.011	0.013	0.024	0.020	0.003	HL91
+ 6451.60	0.26	15495.7	25.40	4.97	0.149	0.244	0.245	0.475	0.403	0.028	-
+ 6460.29	0.20	15474.9	0.79	0.13	0.000	0.007	0.004	0.012	0.009	0.002	-
+ 6491.88	0.15	15399.6	0.76	0.04	0.005	0.019	0.005	0.018	0.018	0.011	-
+ 6494.17	0.21	15394.2	11.17	1.40	0.083	0.114	0.150	0.187	0.200	0.060	-
o 6494.91	0.26	15392.4	1.39	0.51	0.010	0.021	0.009	0.024	0.023	0.009	-
o 6497.55	0.38	15386.2	0.50	0.09	0.004	0.003	0.004	0.007	0.006	0.001	-
+ 6520.70	0.24	15331.5	0.97	0.37	0.005	0.009	0.019	0.030	0.024	0.010	-
+ 6532.10	1.25	15304.8	17.20	1.66	0.238	0.415	0.466	0.622	0.664	0.163	-
o 6536.44	0.11	15294.6	0.69	0.05	0.002	0.004	0.004	0.012	0.008	0.002	-
+ 6591.40	0.53	15167.1	5.55	0.70	0.032	0.057	0.058	0.084	0.087	0.018	-
+ 6597.39	0.05	15153.3	0.72	0.12	0.003	0.014	0.009	0.023	0.019	0.003	H75
+ 6613.72	0.12	15115.9	1.14	0.02	0.064	0.151	0.107	0.326	0.231	0.037	M34
+ 6632.93	0.10	15072.1	1.06	0.16	0.006	0.006	0.012	0.024	0.017	0.006	-
+ 6660.64	0.13	15009.4	0.84	0.18	0.014	0.045	0.010	0.078	0.051	0.029	H67, H75
o 6694.46	0.06	14933.6	0.64	0.14	-1.00	0.003	0.004	0.005	0.005	0.002	-
+ 6699.37	0.11	14922.6	1.15	0.04	-1.00	0.027	0.016	0.063	0.041	0.011	S78, F83, (H75)
+ 6701.98	0.09	14916.8	0.99	0.14	-1.00	0.008	0.009	0.021	0.015	0.002	F83
o 6709.24	0.05	14900.7	1.30	0.20	0.004	0.006	0.004	0.014	0.009	0.002	FD84, W86, HL91
+ 6740.96	0.15	14830.6	0.97	0.33	0.001	0.005	0.013	0.010	0.013	0.009	(H75)
+ 6770.05	0.13	14766.9	0.74	0.15	0.002	0.006	0.011	0.012	0.013	0.006	H88 (H75)
+ 6788.89	0.08	14725.9	0.87	0.25	-1.00	0.004	0.003	0.011	0.007	0.002	H88
+ 6792.45	0.17	14718.2	1.06	0.16	0.005	0.006	0.010	0.021	0.015	0.004	H88
+ 6795.37	0.12	14711.8	0.90	0.08	-1.00	0.005	0.006	0.009	0.009	0.002	H88
+ 6801.41	0.11	14698.8	0.66	0.13	0.001	0.004	0.004	0.010	0.007	0.001	H88
+ 6803.28	0.10	14694.7	0.80	0.20	0.003	0.003	0.004	0.007	0.006	0.001	H88
+ 6811.44	0.38	14677.1	1.50	0.30	0.004	0.012	0.010	0.024	0.018	0.001	H88
o 6812.82	0.29	14674.2	0.80	0.20	0.005	0.010	0.011	0.023	0.017	0.002	H88
+ 6827.28	0.06	14643.1	0.96	0.08	0.003	0.007	0.007	0.027	0.015	0.006	H88
+ 6841.59	0.13	14612.4	0.62	0.06	0.001	0.002	0.006	0.007	0.007	0.004	H88
+ 6843.44	0.05	14608.5	1.18	0.05	0.008	0.016	0.015	0.035	0.027	0.001	H88
+ 6852.90	0.19	14588.3	1.38	0.08	0.005	0.011	-1.00	0.024	0.018	0.001	H88
+ 6860.02	0.14	14573.2	0.93	0.07	0.001	0.016	0.010	0.034	0.024	0.005	H88
+ 6886.92	0.10	14516.3	0.73	0.23	-1.00	0.023	0.021	0.049	0.038	0.001	HL91
+ 6919.25	0.04	14448.4	0.96	0.04	-1.00	0.029	0.040	0.050	0.053	0.016	HL91
+ 6939.00	0.17	14407.3	21.27	3.04	0.138	0.259	0.276	0.353	0.396	0.104	HL91
+ 6944.53	0.08	14395.8	0.84	0.21	-1.00	0.013	0.021	0.033	0.028	0.008	-
o 6978.54	0.06	14325.7	0.81	0.20	0.004	0.005	0.010	0.013	0.012	0.005	-
+ 6993.18	0.09	14295.7	0.96	0.06	0.024	0.073	0.054	0.169	0.116	0.020	HS82
- 6998.71	0.11	14284.4	0.56	0.13	0.001	0.011	0.013	0.009	0.016	0.008	-
o 7045.65	0.25	14189.2	0.84	0.02	0.001	0.006	0.009	0.015	0.013	0.003	-
+ 7060.81	0.32	14158.8	0.67	0.16	0.004	0.006	0.013	0.029	0.019	0.008	-
+ 7062.70	0.10	14155.0	0.60	0.04	-1.00	-1.00	0.013	0.029	0.023	0.000	-
+ 7069.65	0.19	14141.1	0.92	0.09	0.002	0.010	0.012	0.041	0.023	0.009	-
o 7078.02	0.20	14124.3	0.71	0.12	0.009	0.012	0.003	0.018	0.013	0.007	-
+ 7085.10	0.13	14110.2	2.00	0.43	0.014	0.016	0.016	0.043	0.030	0.005	-
- 7099.48	0.05	14081.6	0.40	0.03	-1.00	-1.00	0.004	0.006	0.006	0.002	-
o 7101.14	0.05	14078.4	0.84	0.13	0.005	0.009	0.005	0.010	0.010	0.003	-
+ 7105.93	0.34	14068.9	2.48	0.17	0.027	0.027	0.032	0.034	0.042	0.015	-
+ 7119.94	0.08	14041.2	1.44	0.19	0.009	0.021	0.029	0.044	0.040	0.010	-
+ 7136.09	0.54	14009.4	0.82	0.20	0.005	0.011	0.005	0.013	0.012	0.005	-
+ 7137.97	0.51	14005.7	3.50	0.29	0.012	0.022	0.029	0.060	0.045	0.009	-
o 7153.78	0.17	13974.8	0.67	0.10	0.003	0.002	0.006	0.009	0.007	0.004	-
- 7161.21	0.23	13960.3	2.22	0.35	0.030	0.037	0.045	0.048	0.059	0.021	-
o 7179.95	0.49	13923.8	0.88	0.21	-1.00	0.008	0.015	0.042	0.024	0.011	-
o 7223.13	0.25	13840.6	5.36	0.22	0.023	0.057	0.054	0.078	0.083	0.018	-
+ 7224.18	0.21	13838.6	1.07	0.22	0.054	0.131	0.169	0.333	0.259	0.046	HS82
- 7228.28	0.18	13830.7	0.89	0.27	-1.00	0.011	0.021	0.027	0.026	0.010	-
- 7236.36	0.30	13815.3	0.59	0.20	-1.00	0.007	-1.00	-1.00	0.019	0.010	-
- 7249.26	0.30	13790.7	1.34	0.40	-1.00	0.020	-1.00	-1.00	0.055	0.020	-
- 7257.35	0.30	13775.3	0.61	0.20	-1.00	0.007	-1.00	-1.00	0.019	0.010	-
o 7264.98	0.47	13760.9	1.67	0.87	-1.00	0.019	0.020	0.025	0.029	0.008	-
o 7274.50	0.53	13742.9	5.06	0.52	-1.00	0.029	0.036	0.078	0.058	0.010	-
o 7276.70	0.11	13738.7	1.14	0.37	0.017	0.019	0.034	0.038	0.040	0.017	-
- 7287.62	0.30	13718.1	0.98	0.30	-1.00	0.017	-1.00	-1.00	0.047	0.020	-
- 7302.71	0.30	13689.7	1.99	0.50	-1.00	0.032	-1.00	-1.00	0.088	0.040	-
- 7321.08	0.62	13655.4	1.27	0.29	0.002	0.017	0.014	0.015	0.021	0.008	-
+ 7330.17	0.16	13638.5	1.42	0.47	-1.00	0.015	0.013	0.019	0.021	0.005	-
+ 7334.33	0.12	13630.7	1.24	0.26	0.009	0.034	0.041	0.064	0.060	0.012	HL91
+ 7349.81	0.12	13602.0	0.84	0.32	0.003	0.009	0.008	0.013	0.013	0.002	-
o 7354.92	0.26	13592.6	0.64	0.29	0.002	0.002	0.007	0.011	0.008	0.005	-
+ 7357.20	1.81	13588.4	28.23	2.15	-1.00	0.149	0.152	0.215	0.227	0.049	HL91
+ 7357.60	0.22	13587.6	1.37	0.12	0.010	0.032	0.032	0.043	0.048	0.012	-
+ 7360.45	0.23	13582.4	1.00	0.20	0.007	0.012	0.015	0.021	0.021	0.005	-
+ 7366.61	0.12	13571.0	1.32	0.12	0.015	0.025	0.021	0.062	0.042	0.007	HL91
o 7369.29	0.51	13566.1	1.04	0.08	0.012	0.007	0.017	0.019	0.019	0.010	-
+ 7375.90	0.15	13553.9	0.79	0.39	0.005	0.006	0.011	0.012	0.013	0.006	-
+ 7385.92	0.08	13535.5	0.54	0.11	0.001	0.005	0.004	0.013	0.009	0.002	-
o 7398.58	0.06	13512.4	1.08	0.22	0.013	0.007	0.008	0.012	0.012	0.002	-
o 7401.71	0.50	13506.7	0.98	0.11	0.005	0.005	0.006	0.014	0.010	0.002	-
o 7405.77	0.25	13499.3	0.37	0.11	0.001	0.002	0.004	0.005	0.005	0.002	-
o 7406.35	0.16	13498.2	1.22	0.28	0.006	0.009	0.006	0.020	0.014	0.003	-
+ 7432.07	1.32	13451.5	22.33	0.50	0.182	0.263	0.394	0.654	0.549	0.141	T90, HL91
- 7558.50	0.60	13226.5	1.50	1.00	0.027	0.041	0.006	0.036	0.034	0.027	HL91
+ 7562.24	0.16	13219.9	1.78	0.10	0.018	0.045	0.063	0.096	0.087	0.022	S78
o 7569.70	0.05	13206.9	5.50	0.50	0.011	0.125	0.144	0.266	0.216	0.029	HL91
o 7579.17	0.49	13190.4	1.15	0.11	0.010	0.006	0.012	0.020	0.016	0.006	HL91
+ 7581.24	0.13	13186.8	1.45	0.07	0.027	0.021	0.022	0.044	0.036	0.003	Ga84, HL91
+ 7585.63	0.44	13179.2	0.83	0.20	0.000	0.003	0.009	0.011	0.010	0.006	HL91
+ 7651.37	0.26	13066.0	2.72	0.25	-1.00	0.043	0.052	0.108	0.083	0.012	-
+ 7686.46	0.73	13006.3	3.17	0.99	0.071	0.034	0.049	0.096	0.073	0.017	-
o 7695.92	0.16	12990.3	0.67	0.18	0.007	0.007	0.003	0.014	0.009	0.003	-
+ 7705.90	0.48	12973.5	3.53	0.26	-1.00	0.049	0.056	0.080	0.081	0.018	- -
+ 7709.67	1.53	12967.1	33.53	2.90	-1.00	0.287	0.247	0.540	0.444	0.013	-
o 7713.49	0.28	12960.7	1.29	0.08	0.004	-1.00	0.009	0.017	0.015	0.002	-
+ 7721.03	0.18	12948.1	1.81	0.09	-1.00	0.038	0.041	0.082	0.067	0.006	HL91
+ 7721.88	0.17	12946.6	0.79	0.07	0.004	0.014	0.016	0.022	0.023	0.005	HL91
+ 7748.18	0.72	12902.7	4.53	0.27	0.021	0.040	0.049	0.079	0.072	0.013	-
+ 7782.25	1.58	12846.2	3.64	0.89	0.000	0.049	0.047	0.068	0.072	0.015	-

Table 3. continued

cert	L	err	Nu(cm-1)	FWHM	err	HD30614	21389	190603	183143	W/EB-V	err	cross-reference
+	7832.72	0.06	12763.4	0.84	0.13	0.005	0.017	0.009	0.033	0.023	0.006	HL91
+	7843.87	0.38	12745.3	4.80	0.29	0.029	0.051	0.059	0.074	0.082	0.023	-
o	7862.34	0.10	12715.4	0.67	0.05	0.006	0.006	0.004	0.012	0.009	0.001	-
o	7904.92	0.14	12646.9	1.04	0.36	0.003	0.005	0.012	0.015	0.014	0.007	-
+	7915.13	0.48	12630.6	1.85	0.12	0.007	0.009	0.007	0.038	0.019	0.010	-
+	7927.80	0.44	12610.4	15.00	2.01	0.177	0.227	0.289	0.504	0.428	0.077	T90, HL91
o	7935.33	0.15	12598.4	0.95	0.32	0.006	0.005	0.007	0.014	0.011	0.002	-
o	7987.89	0.21	12515.5	2.90	1.16	-1.00	0.024	0.033	0.069	0.051	0.011	-
+	8026.21	0.15	12455.7	0.79	0.06	0.012	0.026	0.024	0.052	0.042	0.001	HL91
+	8037.24	0.23	12438.7	1.72	0.22	0.009	0.020	0.024	0.045	0.037	0.005	HL91
+	8038.48	0.25	12436.7	3.20	0.10	0.024	0.051	0.045	0.112	0.084	0.006	HL91
o	8283.45	0.18	12068.9	1.21	0.38	-1.00	0.008	0.016	0.052	0.028	0.015	-
+	8530.79	0.38	11719.0	1.73	1.04	0.011	0.029	0.071	0.056	0.073	0.046	-
+	8621.11	0.34	11596.2	1.86	0.24	0.016	0.081	0.078	0.133	0.125	0.016	G76, S78
+	8621.23	0.19	11596.1	5.59	0.52	0.042	0.177	0.158	0.312	0.272	0.018	-
+	8648.28	1.16	11559.8	4.17	1.08	0.045	0.115	0.197	0.233	0.241	0.095	S78

Table 4. Known diffuse bands that were not initially detected in the survey. The reasons for this is indicated. Source: H66 Herbig 1966, H75 Herbig 1975, HL91 Herbig & Leka 1991, S78 Sanner et al. 1978

λ_c	W	τ	FW	ref.	reason
4501.8	0.250	0.065	3.0	H75	*-lines
6307	0.220	0.025	9.	HL91	our 6314
6358.5	0.008	0.010	1.1	HL91	uncertain
6367.26	0.012	0.015	0.8	HL91	we missed this one
6709.5	0.010	0.008	1.3	H66	not obvious in 190603
6767.59	0.010	0.010	1.	H88	not obvious
6803.28	0.006	0.008	1.	H88	weak, but yes
6811.14	0.049	0.024	1.	H88	not in HD 190603
6821.56	0.014	0.008	3.2	H88	missing in 21389
6834.46	0.009	0.010	1.	H88	missing in 190603
6837.71	0.010	0.008	1.	H88	??, ff remnant
6845.31	0.007	0.006	1.	H88	weak, but o.k.
6862.47	0.010	0.010	1.	H88	could be *-line
7405.5	0.117	0.009	15	HL91	3 narrow DIBs
7559.20	0.031	0.016	1.8	HL91	weak in HD 190603
7569.7	0.073	0.014	5.5	HL91	assumed 7564.50
7719.7	0.021	0.022	1.	HL91	shift in λ?
8384	0.086	0.035	2.5	S78	only in HD 183143
8572	0.095	0.013	1.6	S78	*-line

the final catalogue. All the previously known DIBs were included in any case for completeness along with our measurements. We were not able to confirm the two doubtful DIBs listed by Sanner et al. (1978) at 8384 and 8572 Å. Also the 4501.8 DIB by Herbig (1975) is problematic, because of stellar lines in our reference star. However, the interstellar nature of λ4501 has been demonstrated by Morell et al. (1991), and the pattern of lines in the latter structure is different between HD 183143 and βOri, which indicates that this is a bona fide DIB.

Obviously, the DIBs in the catalogue are detected with varying levels of certainty. We give three confidence levels: certain (+), probable (o) and possible (–) interstellar features. In this certainty classification we have adopted the results of other studies. For example, from the sample studied by Jenniskens & Désert (1993) in the 5780 window, we are able to ascertain the presence of the DIB at 5720 Å. On the other hand, the broad DIB at 4590 Å which is strong only in HD 30614 seems to be a blend of stellar lines rather than a DIB (from unpublished spectra of several stars obtained with the same instrument). The confirmation of many of the new DIBs marked "o" and "–" in Table 3 must await further data before they can be marked "+".

4. Results

The data are presented as a catalogue of diffuse bands and a series of plots (Appendix), which allow a better comparison of laboratory data with astronomical observations.

The catalogue (Table 3) contains 229 entries, of which 133 are new (including 19 new detections listed in Jenniskens & Désert 1993). The new entries contain 64 marked certain (+), 52 marked probable (o) and 17 marked possible (–). Three more certain DIBs are known outside the observed window (Sect. 7), which brings the current total of certain DIBs to 157.

The total number of certain and probable DIBs listed in the catalogue is 212, which is about twice the number known before. The possible DIBs contain a number of doubtful cases, but we want to point out that many of the probable DIBs need confirmation too. Also, a small part of the new (certain) detections is due to a decomposition of complex profiles into Gaussian components, in the same way as Herbig (1975). Because we refrain from Gauss fitting, some of these decompositions may not be perfect.

The summation of all equivalent widths results in a total of $W_{\rm DIBs}/E_{B-V} = 22.2$ Å , compared to 13.5 Å for the DIBs listed in Herbig (1975). This value increases to about 25 Å if broad DIBs are present below our sensitivity limit at a similar amount per decade in W as at high values of W. This value does not include DIBs weaker than 0.01 Å, nor the DIBs that are possibly found outside the observed wavelength range.

A discussion of the statistical aspects of the survey, notably the occurence of characteristic shapes and the possible presence of sequences, will be discussed in a separate paper. However, some features of the DIB spectrum are already apparent from the data as presented here.

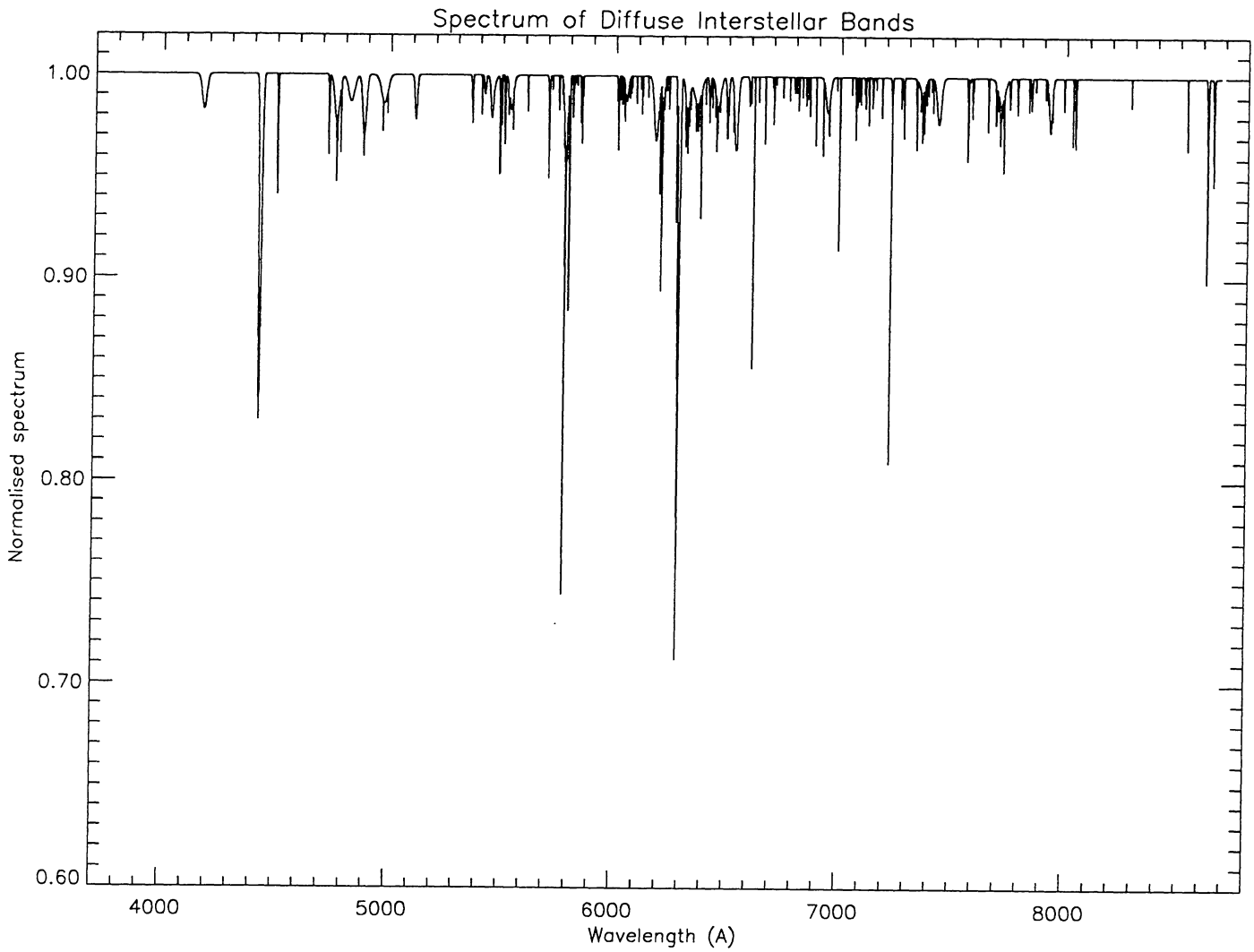

Fig. 4. The DIB spectrum, which is a composite of all certain (+) and probable (o) DIBs listed in the catalogue, smoothed as if observed with a 2 Å resolution instrument and for a line–of–sight of unit reddening

In Fig. 4 we gather the information available in the DIB catalogue of Table 3. Figure 4 is a composite spectrum of the certain and probable DIBs listed in the catalogue made by assuming that the lines are gaussian and that the resolution is 2 Å. It should give a fairly complete picture of the strongest of the DIBs and their distribution in the electromagnetic spectrum. The following features emerge.

DIBs are found mainly between 2.67 and 1.55 eV. The windows above 8000 Å and below 5550 Å are remarkably devoid of narrow DIBs, although a number of complex diffuse bands stand out. A similar multitude of diffuse bands as around 6880 Å is found only between 6000 and 7600 Å. There is some indication of a clustering of narrow lines, although this may reflect sensitivity variations due to abundant telluric lines at some positions in the spectrum.

We report the first (shallow) DIB below 4430 Å at λ4176, which adds to a number of such bands near 5000 Å. The band is present in the low resolution spectra of HD 183143 and Cyg OB2 # 12 given by Souza and Lutz (1980). The band was also noted by Knoechel and Moffat (1982) in HD 80077. We note however that these are both late B type stars and in our survey the band is found at the edge of a window. Some further study is warranted to establish this result. We did not find the large number of bands in the near UV that is expected if the carrier of the DIBs is some set of neutral molecules.

The broadest features that we can detect should have a width of about 50 Å. However, such broad DIBs are not observed. Five DIBs have FWHM in the range 30–40 Å, which are spread all over the spectrum: λ4595, λ4824, λ4970, λ6360 and λ7710. There is a strong selection effect against observing weak shallow bands. Our sensitivity limit is about A_c =0.01, which results in W = 0.01 FWHM. Low resolution observations may lower this limit, but increases the effect of stellar line contamination.

Surprisingly few interstellar absorptions in the visual and near–infrared are as narrow as the instrumental resolution and the Doppler broadening allow. No more than some 25 DIBs have FWHM < 0.70 Å , most of these are very weak DIBs: with W in the range 0.005–0.010 Å and for these the FWHM may well be underestimated. Figure 5 compares the narrowest of the strong DIBs, λ6196 (FWHM = 0.65 Å in our data) with the atomic interstellar KI. The DIB is not split into the cloud components seen in the KI spectra. A comparison of published high resolution data of HD 183143 shows the effect most clearly (i.e. KI data: Gredel et al. 1991, λ6196 data: Herbig & Soderblom 1982). At a resolution of 0.05 Å the DIB is still barely resolvable. This clearly shows that in this particular case the DIB has an intrinsic width. And it suggests that many of the handful of observed narrow DIBs have intrinsic width larger than the Doppler broadening. There is no gradual transition from diffuse interstellar bands to interstellar absorption lines.

And, finally, a more speculative observation: in some windows in the red the random noise between individual spectra seems to correlate, which may indicate the presence of many weak DIBs, if not due to flat fielding remnants. Structure is sometimes infered, for example on top of the 6177, 7432, 6939 and possibly 4430, where we find several weak DIBs at the 1σ level. A thorough analysis of the shallow features around the prominent λ5780 and λ6284 is given by Jenniskens & Désert (1993). Further studies are needed to make sure whether stellar lines (4430) or atmospheric lines (6939, 7432) could be the source of the features in these other bands.

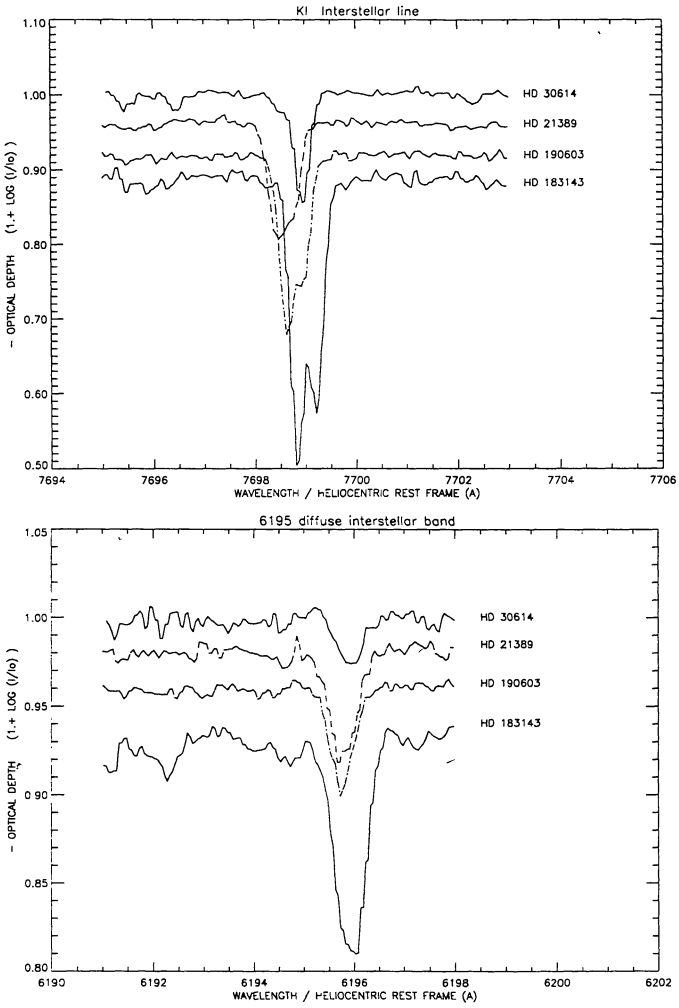

Fig. 5. Interstellar absorption lines of KI at 7699 Å and the narrow DIB at 6196 Å . The lines are plotted as 1-τ in an heliocentric velocity system. Note that each of the KI lines is composed of several cloud components that cannot be discerned in the λ6196 data

5. The use of the survey, an example

This survey is intended to allow for a direct comparison of laboratory spectra of relevant DIB carrier candidates with astronomical data. We will now show an example of how the survey may be used, from one recently proposed candidate: the naphtalene ion (Salama & Allamandola 1992a,b)

Table 6 summarizes data on the oscillator strength and position of the strongest bands of this ion reported by Salama & Allamandola (1992b). We have found two new DIBs very close to the positions that are given. The strongest band of the Naphtalene ion coincides within the observational error with a DIB at 6740.96 ±0.15 Å . This band was listed as 'possible interstellar' in Herbig (1975). Three other slightly weaker bands are present in the laboratory spectrum. One band is predicted at 6520 Å. This band is listed in the catalogue as a new discovery located at 6520.70 ±0.24 Å .

Arguments in favour of an association are the fact that the FWHM of λ6741 and λ6520 is the same (0.97 Å) and the close proximity of laboratory wavelength and DIB position. But the relative intensity of both lines is different from the laboratory measurements, with λ6520 being the strongest instead of λ6741. The relative intensity of the bands may, however, be affected by the matrix as e.g. the band at 6520 Å is identified with a vibronic out of plane bending mode, while the 6741 is thought to be a vibrationless transition (Salama & Allamandola 1992b).

Even then, the identification isn't fully established. The other two predicted bands at 6151 Å and 5965 Å are not present in the catalogue. The band at 5965 Å is obscured by a stellar line, which is present in βOri and strong in HD 21389. (Similarly, the 4560 band is in a region with many stellar lines.) Inspection of the plots reveals that the 6151 should be detected if stronger than $W = 0.008$ Å. Assuming that W_{6741}/E_{B-V} equals 0.020 in the diffuse medium and the FWHM of all bands are the same, the other bands should have strengths of about 0.005, 0.005 and 0.003 Å for λ6520, λ6151 and λ5965 respectively (all bands are optically thin, as a result of which W is proportional to the oscillator strength). If the naph-

talene contributes significantly to λ6741, then the bands at λ6151 and λ5965 should be detectable in observations at somewhat higher signal–to–noise. Snow (1992) reports on an attempt to detect λ6151 and puts a tight upper limit to $W < 0.9$ mÅ .

Note that the width of the lines (FW – Table 5) measured in the laboratory are always larger than observed. This is not a strong objection to identification, because the solid Ne matrix used in the laboratory measurements broadens the line width by internal vibrational conversion.

Table 5. Laboratory signature of the naphtalene ion and the identification in the DIB survey. Laboratory band positions in a Neon matrix. The expected value of the equivalent width (W_{lab}) was computed by multiplying the published oscillator strength by 50, thus scaling the values to the observed equivalent width (W_{obs}) of λ6520 and λ6741. All parameters are in Å

Lab: λ	FW	W_{lab}	ISM: λ	FW	W_{obs}	remarks
4560	29	0.001	-.-	-.-	<0.00..	*-lines
5965	28	0.0025	-.-	-.-	-.-	*-line
6151	38	0.005	-.-	-.-	<0.008	not det.
6520	43	0.005	6520.7	0.97	0.024±0.010	new
6741	54	0.020	6741.0	0.97	0.013±0.009	confirmed

6. Discussion of uncertainties

The identification of DIBs from the plots in the catalogue is not straight forward because, apart from random noise in the data, there is the presence of several kinds of spurious absorptions. These need to be recognized in order to be able to judge the quality of an identification.

6.1. *Random noise*

The random error in the equivalent width due to photon and readout noise is:

$$\Delta W = \mathrm{rms}\sqrt{(2\,\Delta\lambda\ \mathrm{FWHM})} \qquad (5)$$

where rms refers to the root mean square of the normalised signal in a featureless continuum per pixel of 0.1 Å. Figure 1 shows this random error in a typical DIB of FWHM = 1 Å . The thick line is an estimated sensitivity limit, which is taken to be the random noise of any set of two stars with highest S/N, but including HD 190603 or HD 30614 in order not to be misguided by the similarity in spectral type of HD 21389 and HD 183143. This sensitivity limit is nearly constant over a wide range of the spectrum and decreases by a factor of two for $\lambda < 4580$Å and $\lambda > 8140$Å

Occasionally one of the four stars has a lower signal–to–noise in a window as a result of unfortunate weather conditions during the observations. HD 183143 is not well observed below $\lambda = 4580$ Å , because of the strong extinction of interstellar dust. This is compensated for by a high signal to noise in HD 30614.

The actual error in W depends on the accuracy at which the baseline can be placed (and the presence of contaminating stellar and telluric lines) and is therefore larger than indicated. We found that at best a 1 Å DIB of $W/E_{B-V} = 0.008$ Å could be detected, which is about $3\Delta W$.

6.2. *Spurious absorptions*

Other sources of absorption include stellar lines, telluric lines, and remnants of the detector sensitivity profile. Stellar line contamination is heavy below 4700 Å and in the 8400 Å window (due to the Paschen series of hydrogen). On the other hand, because of the high wavelength resolution, weak stellar lines do not seriously limit the possibility of detecting a narrow DIB.

Remnants of telluric lines are present in the regions between: 6866–6918 Å (due to oxygen), 7164–7300Å (water), 7594–7660 Å (oxygen) and between 8130–8240 Å (water), which cover about 12% of the survey. Telluric line remnants are due to small shifts of the spectrum on the CCD during the exposure, or due to non perfect matching of the wavelength position of program and reference star after a change of central position. Worst in this respect are HD 34085 and HD 30614, which unlike other stars are not observed by pair exposures. On the other hand, a very good telluric line removal was possible for HD 21389 in the window containing 7220–7350 Å. The spectrum was obtained at a time when the spectrograph was very stable. From this spectrum we identify 5 absorption features, listed in Table 3 as possible (–), which, unfortunately, cannot be identified as DIBs with the help of other spectra.

Features that originate from the pixel–to–pixel sensitivity variation of the detector are shown in Fig. 2. These are examples of typical flat fielding calibration spectra. Notably a broad depression near pixel 600, of width FWHM = 3.8 Å, in the early Sept. '90 observations may easily be misidentified.

Usually, the intensity of the Th–Ar wavelength calibration lamp could be set in such a way that the emission lines do not saturate. In several windows above 7500 Å this was not possible, because of the dominance of one Thorium or Argon line. Hence, we expect ghost images at 6967, 7068, 7384, 7634, 7726, 7947, 7966, 8007, 8016, 8105, 8119, 8265, 8417 and 8446 Å, but only in one or two instances such a remnant is suspected.

Note that by splitting the detection and reading device, the occurence of ghost images from strong stellar or telluric lines is suppressed to a point where none can be detected (Gillet 1990).

6.3. *Wavelength calibration*

Wavelength calibration errors are typical of order 0.05 Å. The random error in λ_c is somewhat larger and depends on the S/N in the feature. From a comparisson with Jenniskens & Désert (1993), we estimate this value of order 0.2 Å . Individual errors may be as high as 0.6 Å . Notably the windows at 7320 (10), 7680 (9), 8220 (10), 8400 (10) and 8580 (6) have ten or less calibration lines in the Th–Ar calibration lamp spectrum. In other windows the band edges are not well covered by calibration lines and a (second order polynomial) extrapolation is applied. These uncertainties limit the possibility of using the radial velocity difference between stellar lines and interstellar absorption bands as a criterion for discriminating between both. Note that the error is usually confined to one wavelength window. If an error occurs for a band at given wavelength, all lines in part of that band may be shifted.

6.4. *Other limitations: broadening*

There is intrinsic broadening in the absorption lines due to multiple cloud components in the line of sight. These cloud components are apparent in the profile of the interstellar KI absorption line at 7699 Å (Fig. 5). The Doppler broadening is strongest in HD 190603 and HD 183143 and, after convolution with the instrumental passband, results in a FWHM of 0.6–0.7, which makes it more difficult to discriminate between DIBs and more narrow lines of atoms and small molecules. More suitable for this purpose are HD 21389 and HD 30614, which give a minimum FWHM resolution of some 0.47 Å (Table 1). The averaging proceedure involved in deriving the data in Table 3 limits the FWHM resolution to about 0.65 Å , i.e. λ6196, which has an intrinisc width of 0.4 Å(Hayden–Smith et al. 1981; Herbig & Soderblom 1982).

The stellar lines of HD 190603 and HD 183143 have widths similar to those of a large number of DIBs ($\sim$ 1.0 Å). On the other hand, the stellar lines of HD 21389 are significantly narrower (0.65±0.06 Å) and DIBs of width $\sim$1Å stand out best in this spectrum.

7. Prospects for more DIBs to be found

The finding of a laboratory absorption feature that is masked by a stellar line in our spectra, should not be an objection for trying new observations. A good subtraction of the stellar component is in principle possible when pairs of stars are observed with the same spectral type but different reddening. It is necessary, however, to take stars with similar projected stellar rotational velocity, similar composition, and similar stellar wind features and such ideal pairs are difficult to find. It is also possible to obtain a better atmosphere removal, which demands a stable spectrometer. Short integration times are preferable. Atmospheric line removal can be improved by increasing the resolution of the spectra to, say, 0.05 Å, which is quite feasible with some of the modern spectrographs.

What are the prospects for further searches of DIBs? Although there are no diffuse bands known at wavelengths shorter than 3800 Å (Seab & Snow 1985), diffuse bands are certainly to be found at longer wavelengths. Two bands were found by Joblin et al. (1990) as far out as λ = 1.18 and 1.32 μm. There is also a possible DIB reported amongst the C_2 lines at 8764.2 Å (Gredel & Münch 1986). These data are summarized in Table 6. We will now discuss the depth of existing studies and the possibilities of future new finds.

In the near UV, confusion due to stellar lines is a serious limitation to finding new DIBs. There also seems to be a lack of narrow DIBs at these high frequencies and the chance of finding more DIBs is small. Herbig searched below 3800 Å, down to 3350 Å, without success (Herbig 1967). Seab and Snow (1985) searched in the IUE data (1300–3300 Å) for broad features without success, but these data are only of 7 Å resolution and have low signal–to–noise. S/N is of order 24 in continuum extinction for the short wavelength window, IUE–SWP, and S/N = 13 in the long wavelength window IUE–LWP. The strong λ4430 would only just be detectable. In the near–future, the Hubble Space Telescope could bring more information in this spectral window.

Table 6. Previously known DIBs that are outside the wavelength boundaries of the present DIB survey

λ	FWHM	W/E_{B-V}	references
8763.45	0.52	0.010	Gredel & Münch 1986
11797	2.7	0.048	Joblin et al. 1990
13175	4.0	0.097	Joblin et al. 1990

In the near IR, there are certainly prospects for finding new DIBs, although our data indicate that the number of DIBs per unit wavelength interval tends to decrease (see Ehrenfreund et al. 1994). The window between 8745 and 8815 Å, which is just outside our survey, has been well studied because of the presence of the (2,0) bands of the Phillips ($A^1\Pi_u - X^1\Sigma_g^+$) system of C_2. Notably van Dishoeck & de Zeeuw (1984) obtained a number of spectra of highly reddened stars with $\Delta\lambda$ = 0.11 Å at a S/N that would give an error in W/E_{B-V} of an amazing 5 10^{-4} Å. Gredel & Münch (1986) noted that an absorption below the $Q(4)$ line is probably a DIB (λ8763). The data of van Dishoeck & de Zeeuw (1984) show an additional broad absorption centered at 8802±2 Å , FWHM $\sim$ 12 Å , A_c = 0.019 and W/E_{B-V} = 0.245. The feature is most conspicuous in HD 147889, the most reddened star. However, the spectrum of HD 148184 (χ Oph) shows a broad and strong band between 8790 and 8804 Å in spite of a low reddening. At least some features seen in the struc-

ture are due to flatfielding remnants. This structure needs confirmation. No other candidate DIBs are found. Sanner et al. (1978) searched up to 8900 Å at low S/N with no strong DIBs found.

At higher signal–to–noise ratio, more DIBs are definitely to be found in the wavelength range covered by this survey. Such high signal–to–noise is not unfeasible. Many DIBs reported here as probable or possible await confirmation.

Acknowledgements. We are indepted to Dennis Gillet, Pascale Ehrenfreund and Bernard Foing for giving us some of their observing time and for sharing the enthousiasm that was needed to finish the project. Harm Habing and Michel Dennefeld have made these observations possible. The paper benefitted from discussions with Xander Tielens.

References

Aiello S., Barsella B., Chlewicki G., Greenberg J.M., Patriarchi P., Perinotto M. 1988, A&AS 73, 195
Beals C.S., Blanchet G.H. 1937, PASP 49, 224
Benvenuti P., Porceddu I. 1989, A&A 223, 329
Chlewicki G. 1985, Observational constraints on multimodal Interstellar Grain Populations, Thesis Leiden University
Chlewicki G., de Groot M.S., Van der Zwet G.P., Greenberg J.M., Alvarez P.P., Mampaso A. 1987, A&A 173, 131
Crawford M.K., Tielens A.G.G.M., Allamandola L. 1985, ApJL 293, L45
Désert F.–X., Jenniskens P., Dennefeld M. 1994, A&A, in press
van Dishoeck E.F., de Zeeuw T. 1984, MNRAS 206, 383
Ehrenfreund P., d'Hendecourt L., Verstraete L., Léger A., Schmidt W., Defourneau D. 1992, A&A, 259, 257
Ehrenfreund P. et al. 1994, A&A, in preparation
Ferlet R., Roueff E., Horani M., Rostas J. 1983, A&A 125, L5
Ferlet R., Dennefeld M. 1984, A&A 138, 303
Fitzpatrick E.L. and Massa D. 1988, ApJ 328, 734
Gammelgaard P. 1984, A&A 135, 77
Geary J.C. 1976, in Proc. IAU Coll. 40, eds. M. Duchesne and G. Lelièvre, p. 28–1
Gredel R., Münch G. 1986, A&A 154, 336
Gredel R., van Dishoeck E.F., Black J.H. 1991, A&A 251, 625 – unpublished high resolution spectrum of HD 183143
Gillet D. 1990, Manual of the Aurelie spectrograph
Hayden–Smith W., Snow T.P., Jura M. and Cochran W.D.S. 1981, ApJ 248, 128
Heger M.L. 1992, Lick Obs. Bull. 10, 146
Herbig G.H. 1966, Z. Astrophys. 64, 512
Herbig G.H. 1967, in Radio Astronomy and the Galactic System, IAU Symp 31, ed. H. van Woerden, p. 85
Herbig G.H. 1975, ApJ 196, 129
Herbig G.H. and Soderblom D.R. 1982, ApJ 252, 610
Herbig G.H. 1988, ApJ 331, 999
Herbig G.H. and Leka K.D. 1991, ApJ 382, 193
Hobbs L.W. 1984, ApJ 280, 132
Jenniskens P. and Greenberg J.M. 1993, A&A 274, 439
Jenniskens P. and Désert F.–X. 1993, A&A 274, 465
Jenniskens P., Ehrenfreund P., Foing B. 1993, A&A, in press
Joblin C., Maillard J.P., d'Hendecourt L., Léger A. 1990, Nature 346, 729
Knoechel G. and Moffat A.F.J. 1982, A&A 110, 263
Léger A., d'Hendecourt L. 1985, A&A 146, 81
Middleburg F. 1981, IHAP User's Manual
Merrill P.W. 1934, PASP 46, 206
Moore C.E. 1972, A multiplet table of astrophysical interest, NSRDS–NBS 40, National Bureau of Standards
Morell N., Walborn N.R., Fitzpatrick E.L. 1991, PASP 103, 341
D'Odorico S., la Dous C., Ponz D., Tanné J.L. 1984, An Atlas of the Thorium–Argon spectrum for the ESO Echelle Spectrograph, ESO internal publication
Salama F. and Allamandola L.J. 1992a, Nature 358, 42
Salama F. and Allamandola L.J. 1992b, ApJ 395, 301
Sanner F., Snell R., Vanden Bout P. 1978, ApJ 226, 460
Seab C.G., Snow T.P. 1985, ApJ 295, 485
Snell R.L., Vanden Bout P.A. 1981, ApJ 244, 844
Snow T.P. 1992, ApJ 401, 775
Snow T.P., York D.G. and Welty D.E. 1977, AJ 82, 113
Souza S.P., Lutz B.L. 1980, ApJ 235, L87
Torres–Dodgen A.V. 1990, PASP 102, 1406
Van der Zwet G. 1987, in Polycyclic Aromatic Hydrocarbons and Astrophysics, eds. Léger et al., (Reidel: Dordrecht) p. 351
Van der Zwet G., Allamandola L.J. 1985, A&A 146, 76
Wu C.–C., York D.G., Snow T.P. 1981, AJ 86, 755
Wilson R. 1958, ApJ 128, 57

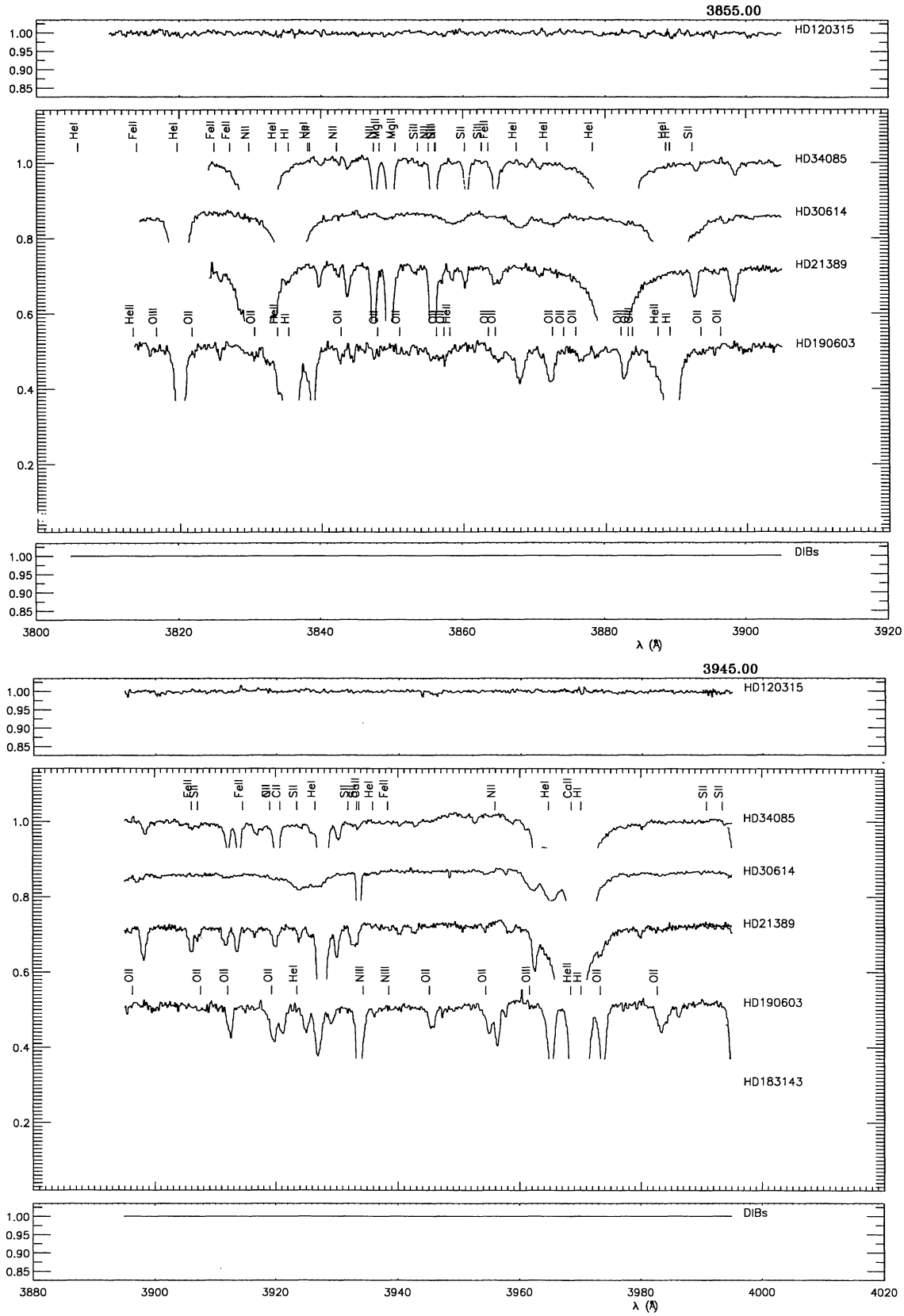

Fig. 6. Appendix: From top to bottom, spectra of atmospheric contamination, an unreddened stellar line reference B8Ia star, a series of four reddened stars in order of increasing reddening shifted by an arbitrary amount in the vertical direction, along with a synthetic DIB spectrum. The DIB spectrum is an expansion of Fig. 4 at full resolution, scaled to the reddening of HD183143 ($E_{B-V} = 1.28$), and is a composite of Gaussian line shapes with mean parameters as in Table 3. Dotted lines in the DIB spectrum correspond to possible but uncertain DIBs (Table 3 marked –). Vertical bars show the location of a selection of stellar lines from Moore (1972) in late B–type stars (top row) and early B–type and late O–type stars (bottom row). Some data, in particular around strong emission or absorption lines, are clipped for easier reading

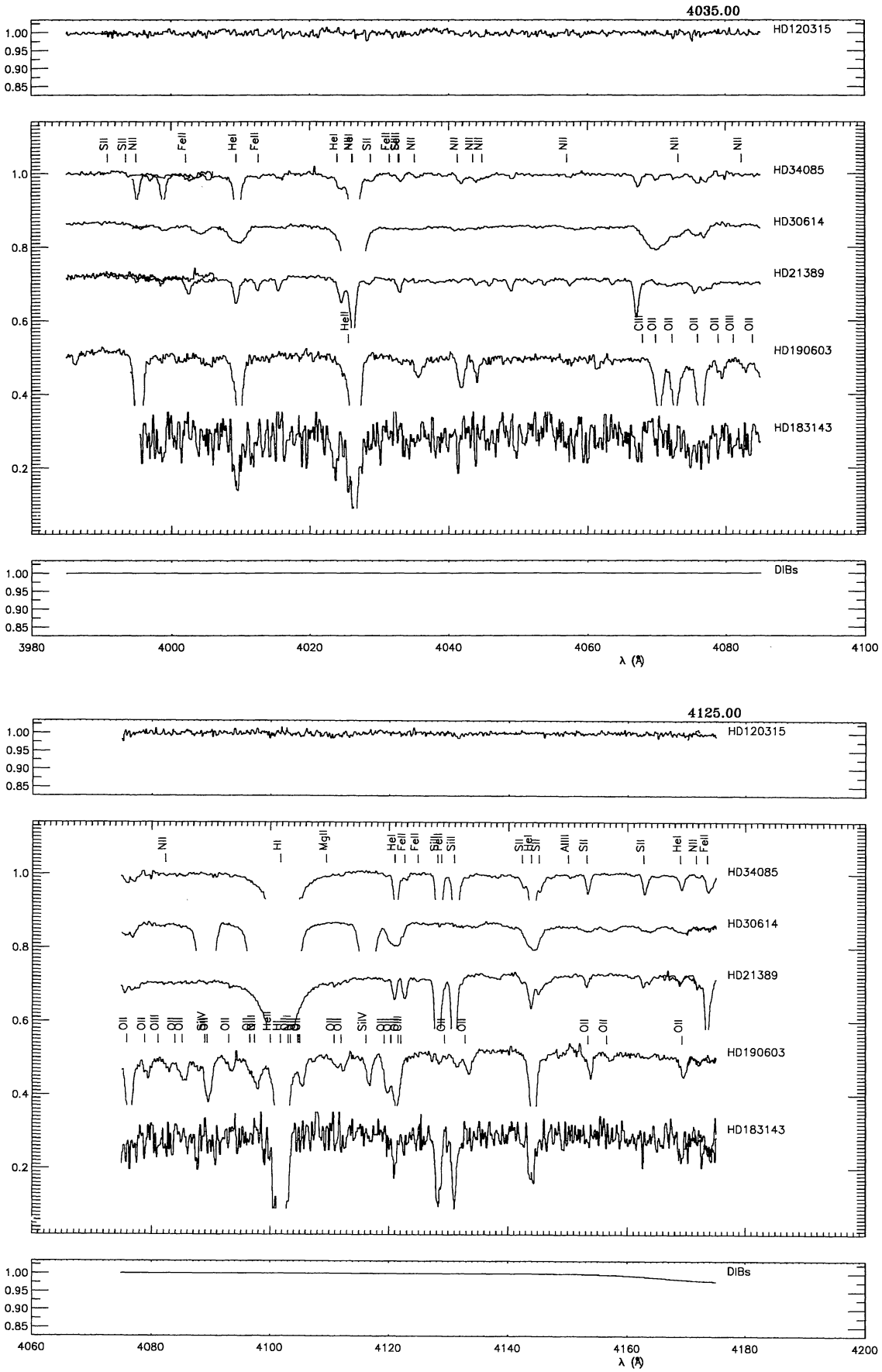

Fig. 6. continued

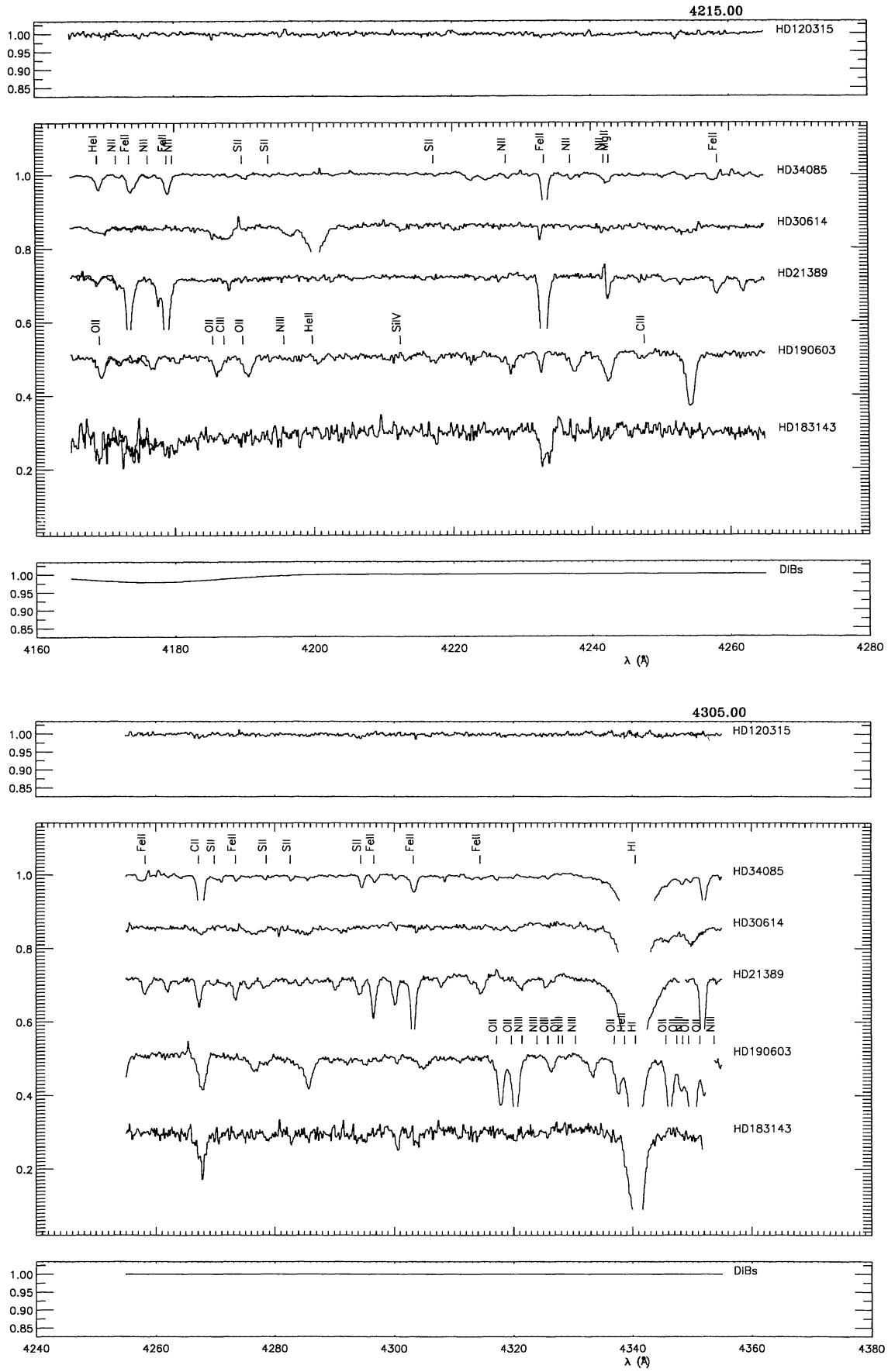

Fig. 6. continued

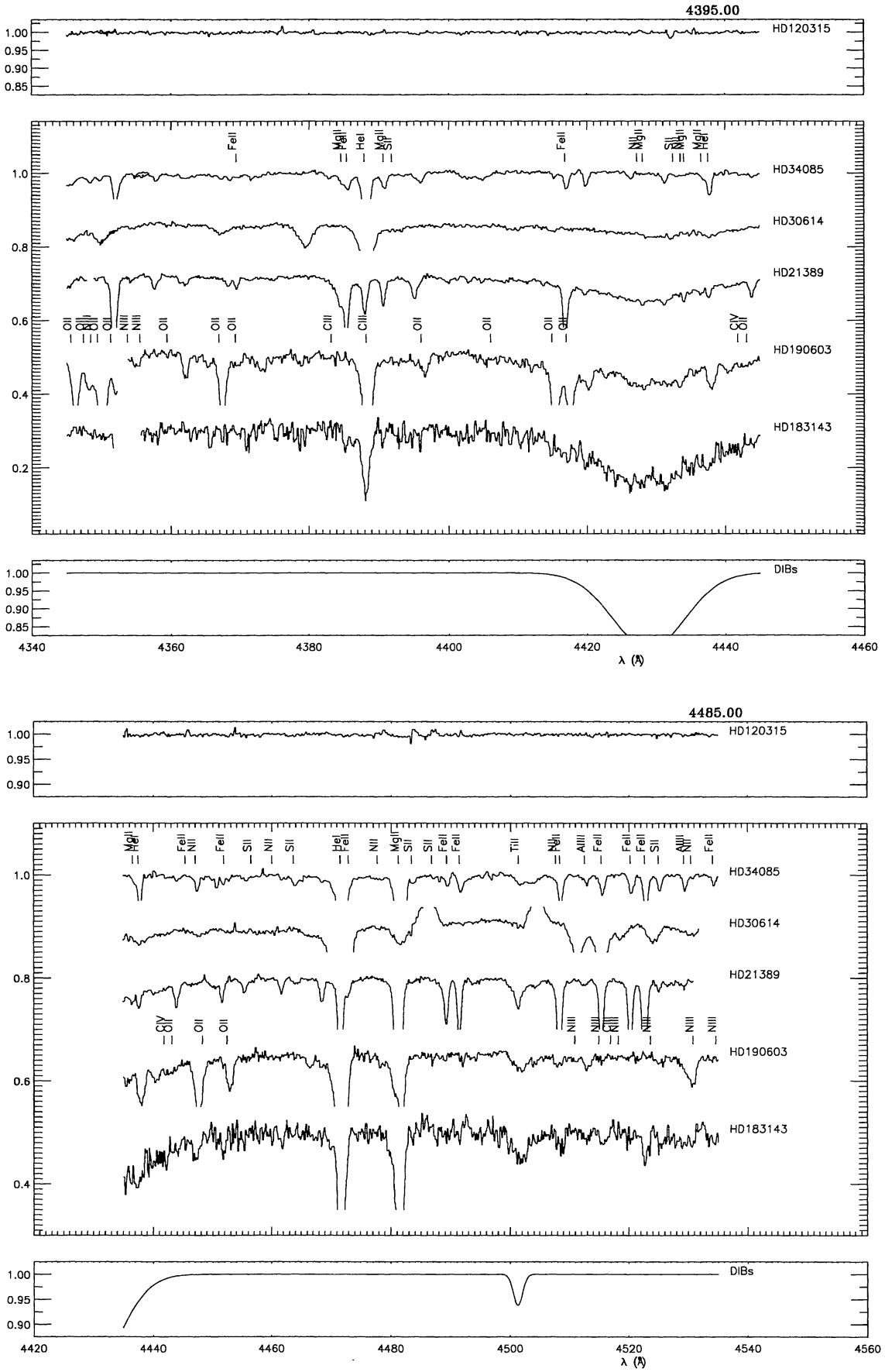

Fig. 6. continued

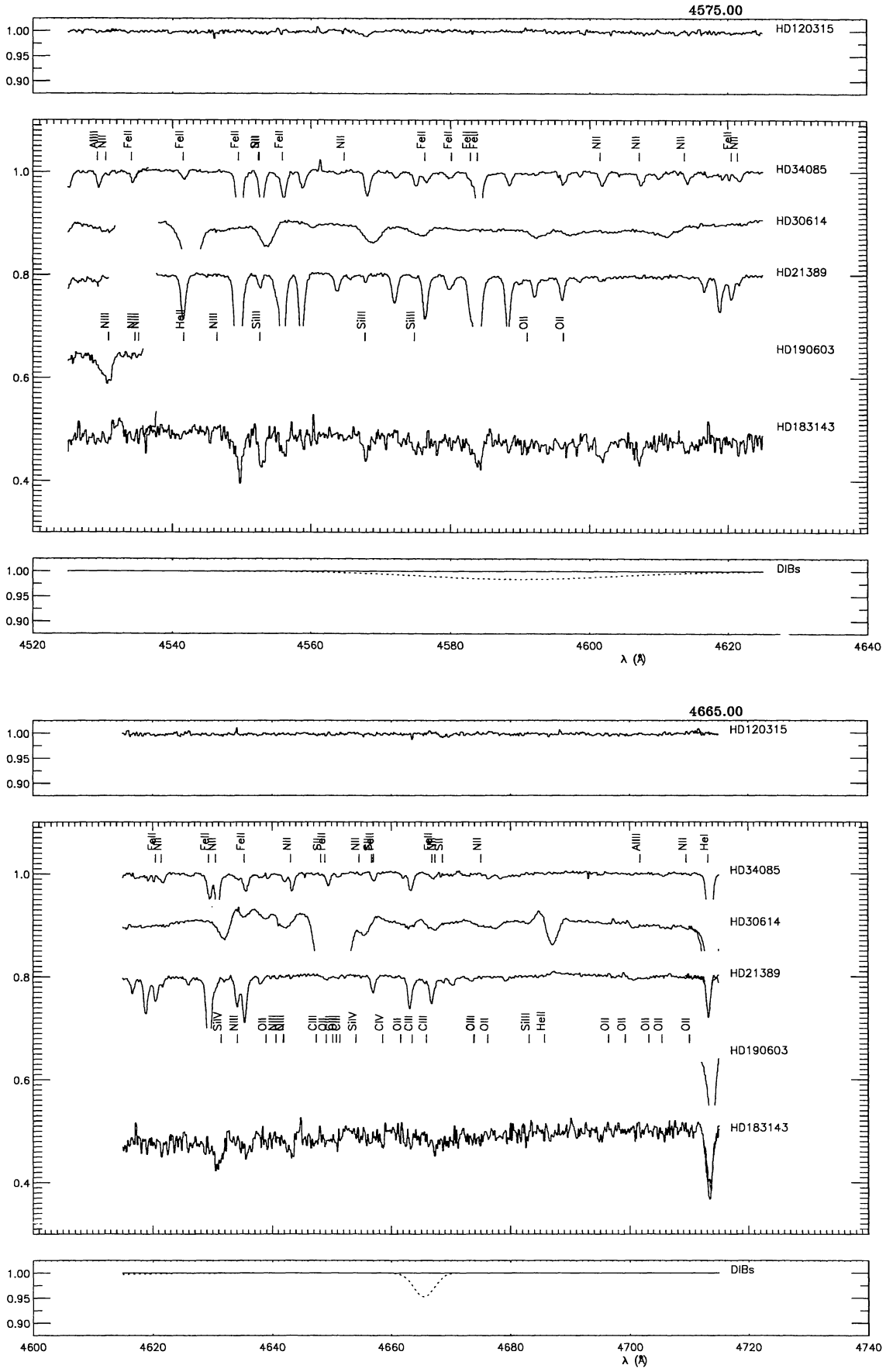

Fig. 6. continued

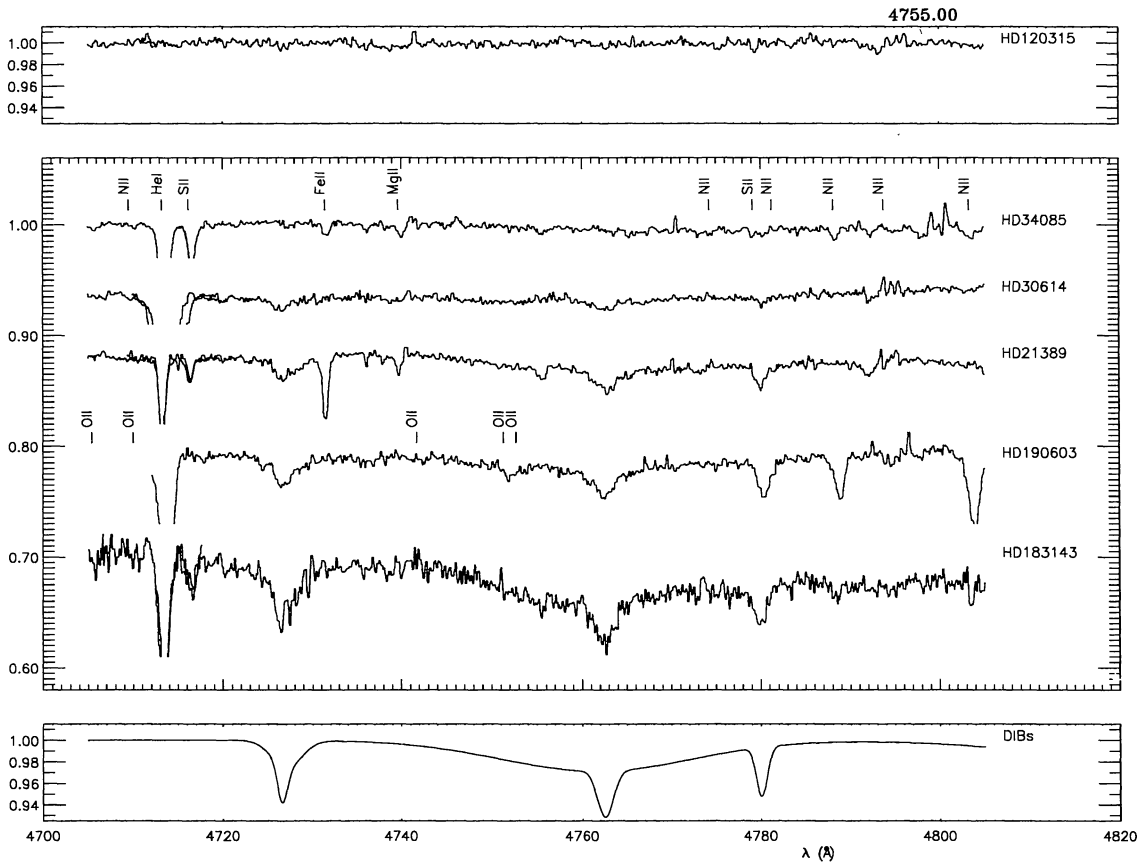

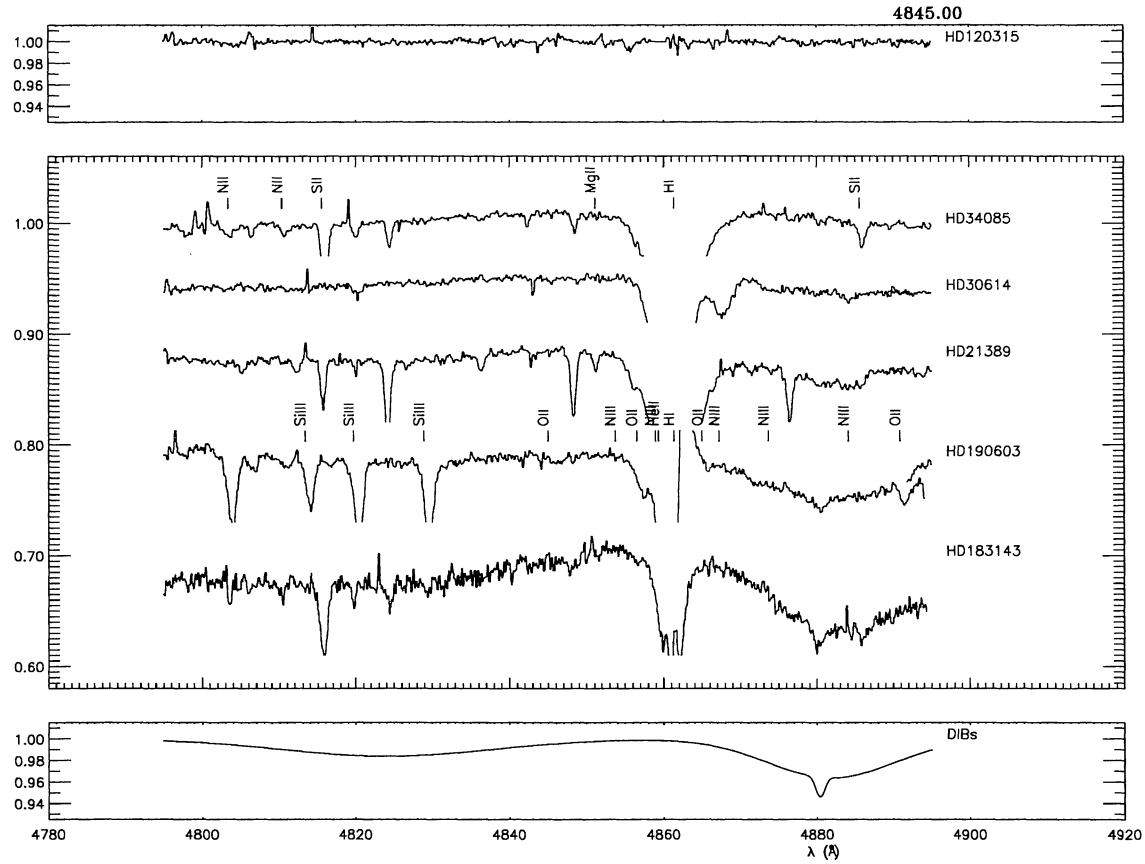

Fig. 6. continued

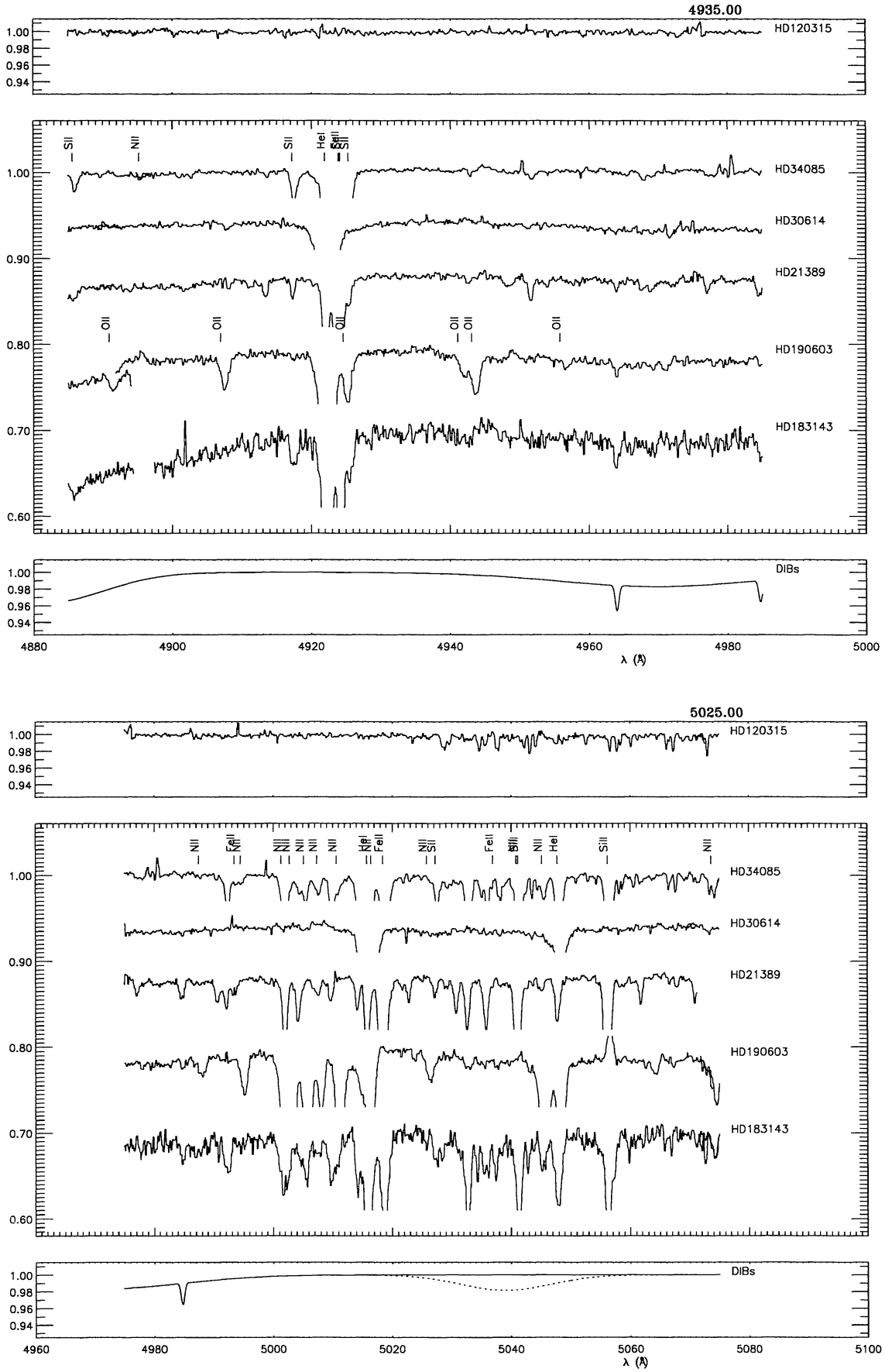

Fig. 6. continued

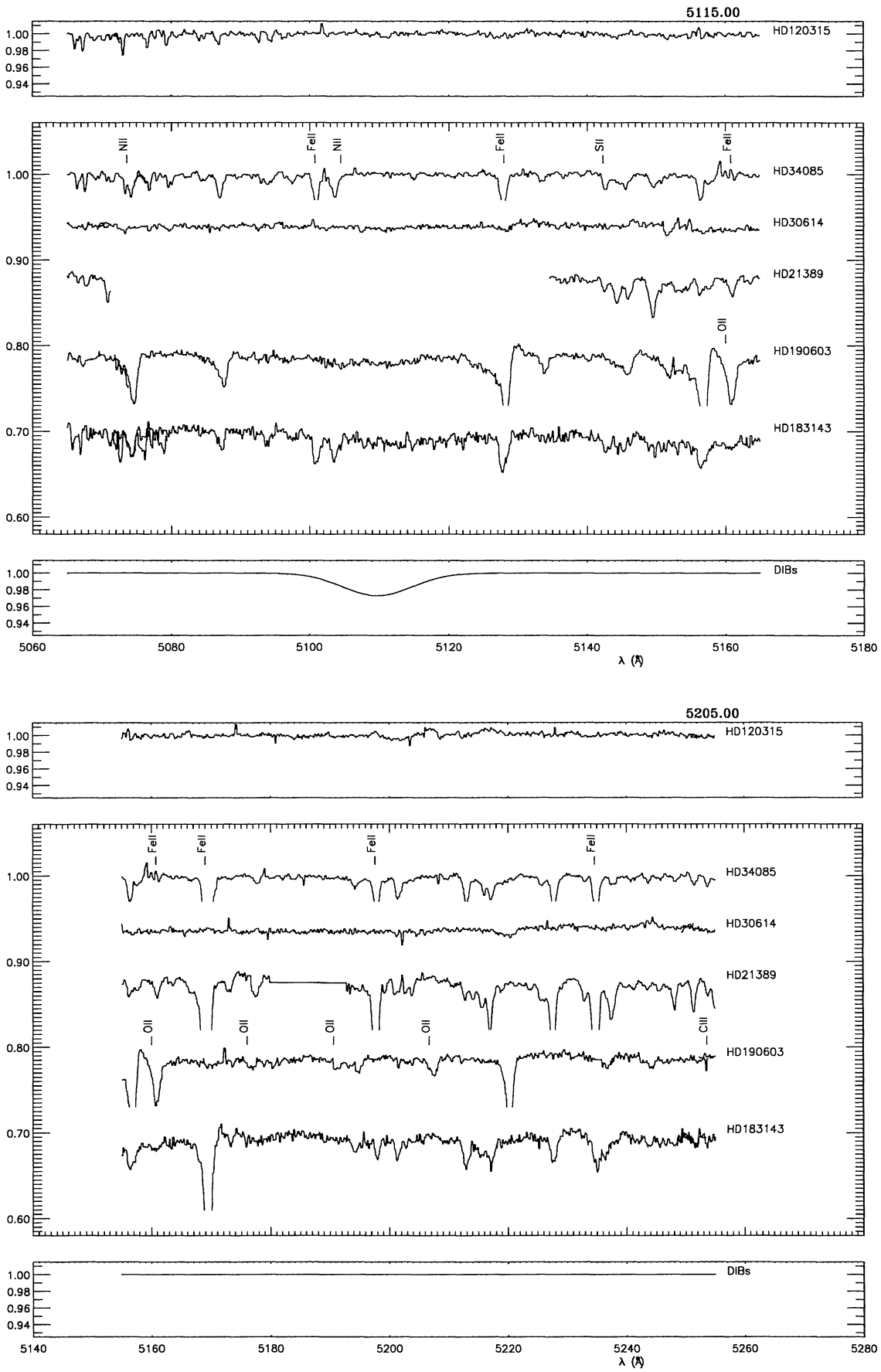

Fig. 6. continued

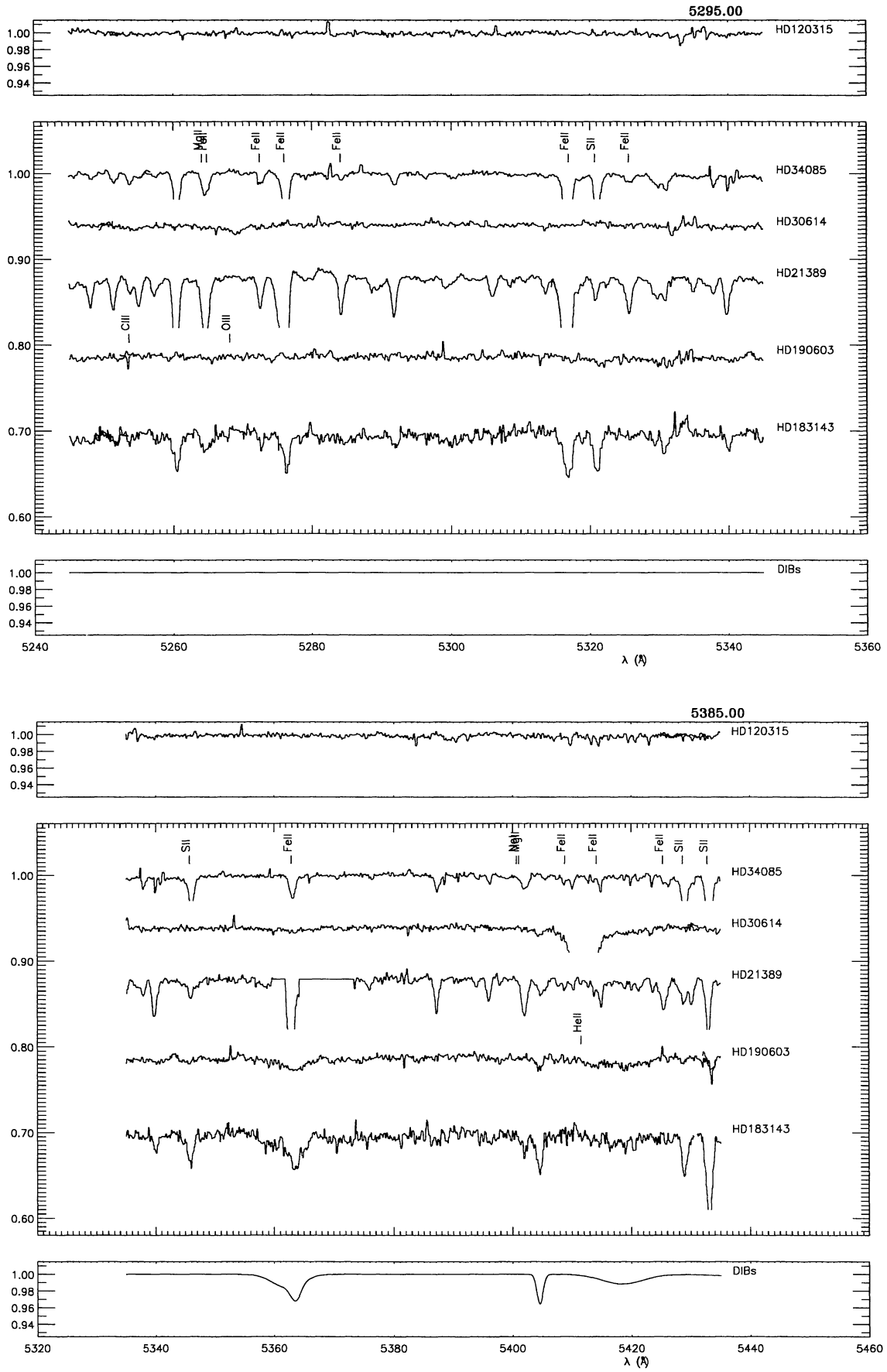

Fig. 6. continued

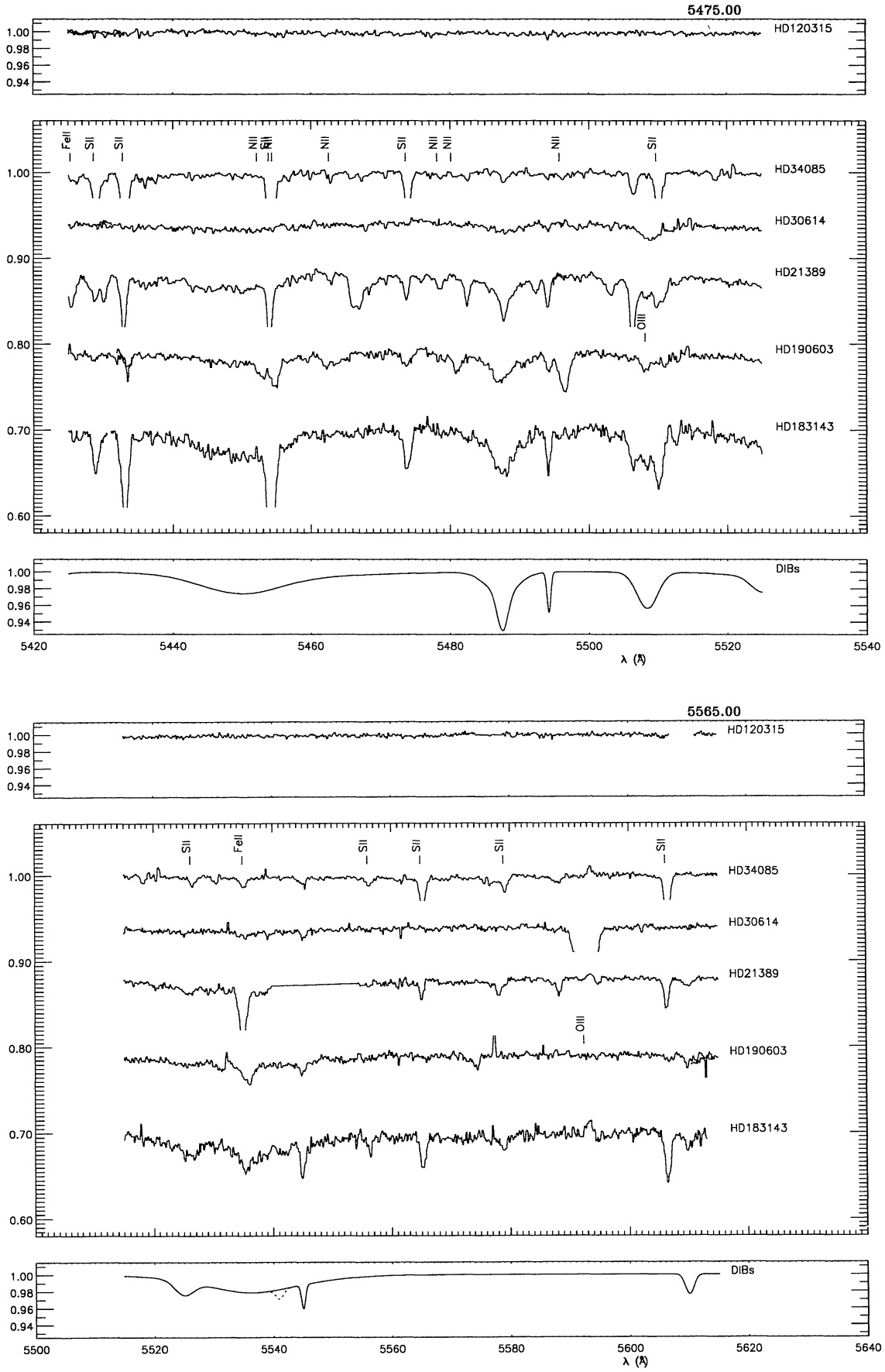

Fig. 6. continued

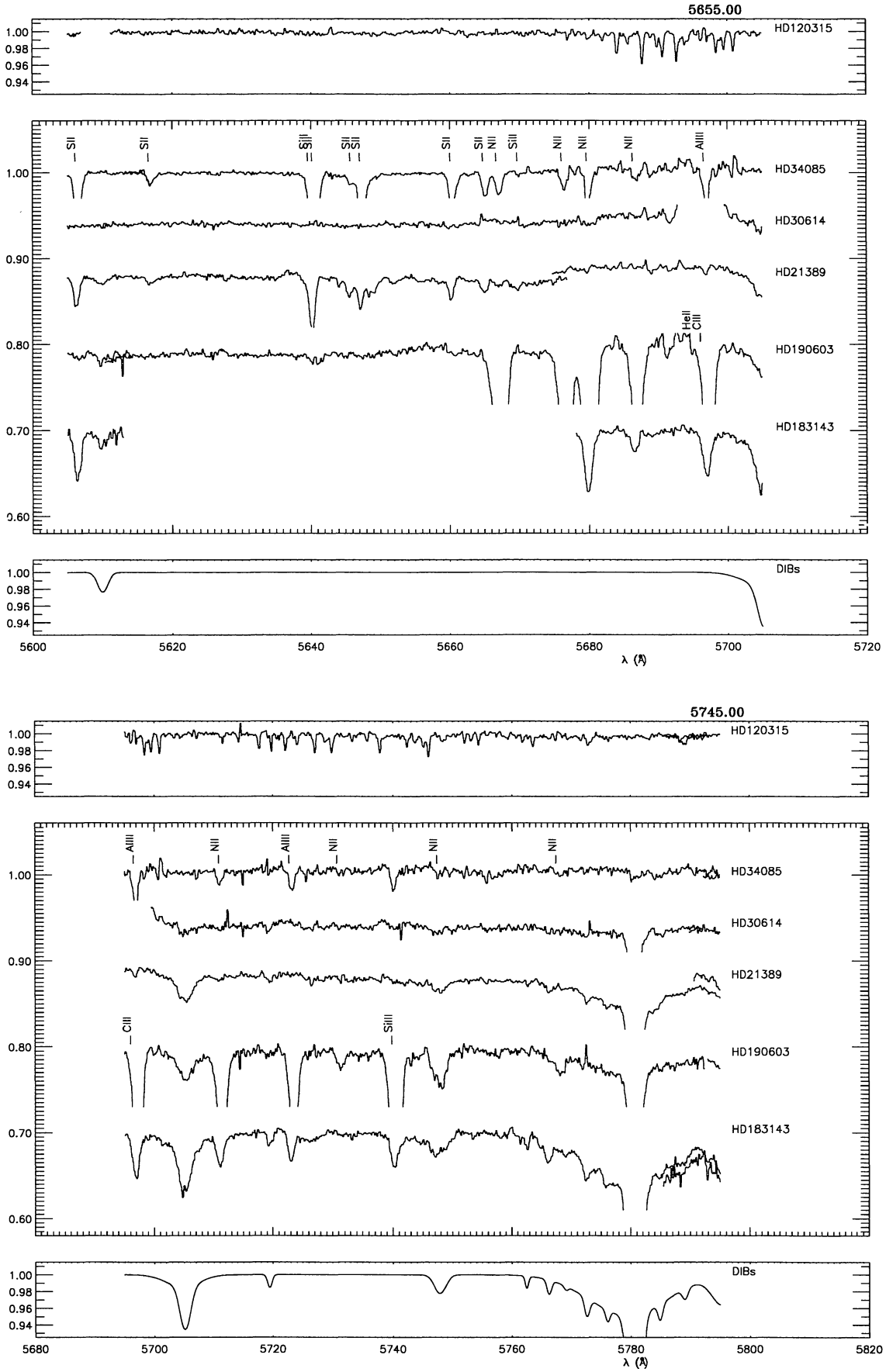

Fig. 6. continued

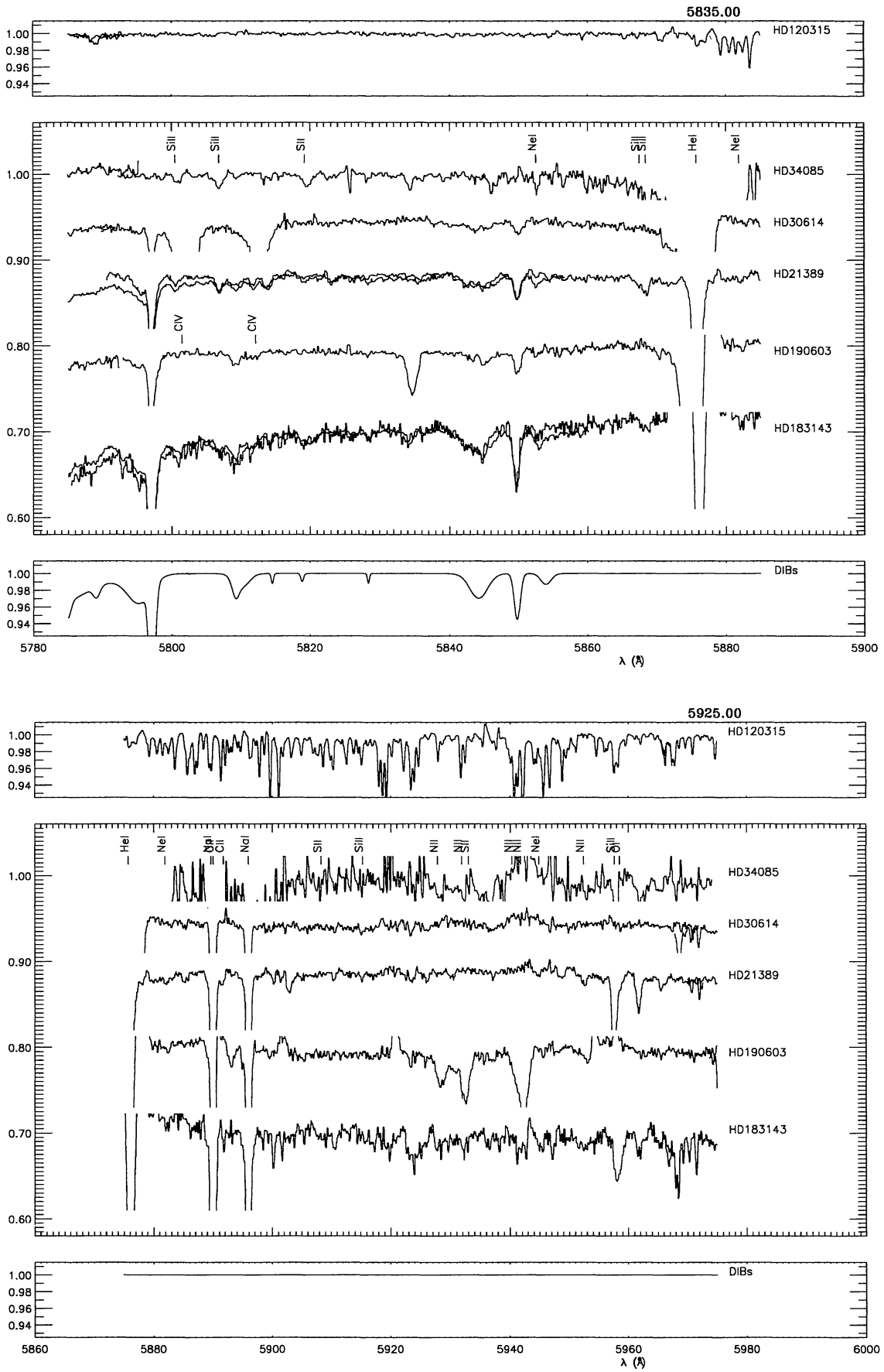

Fig. 6. continued

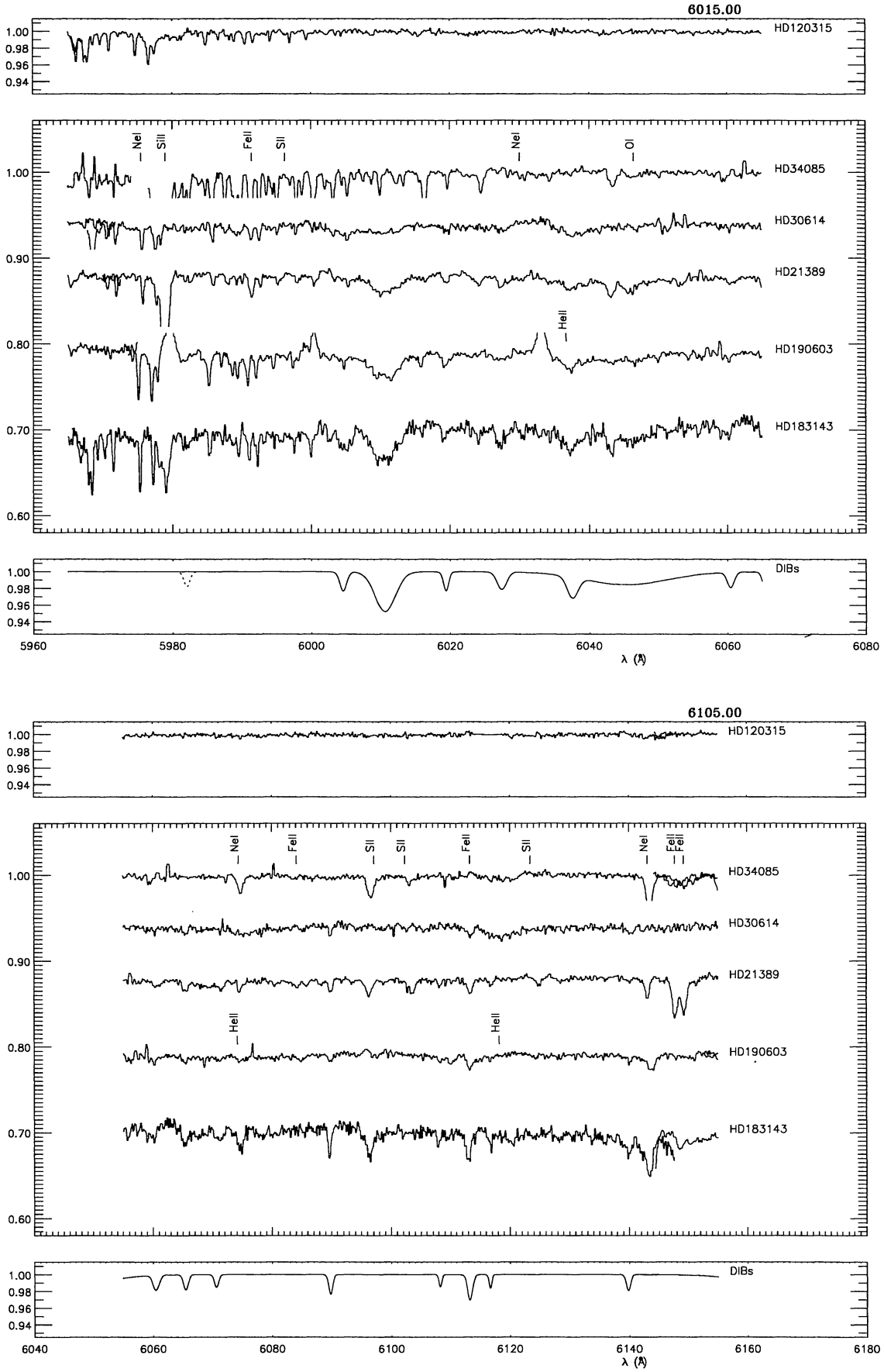

Fig. 6. continued

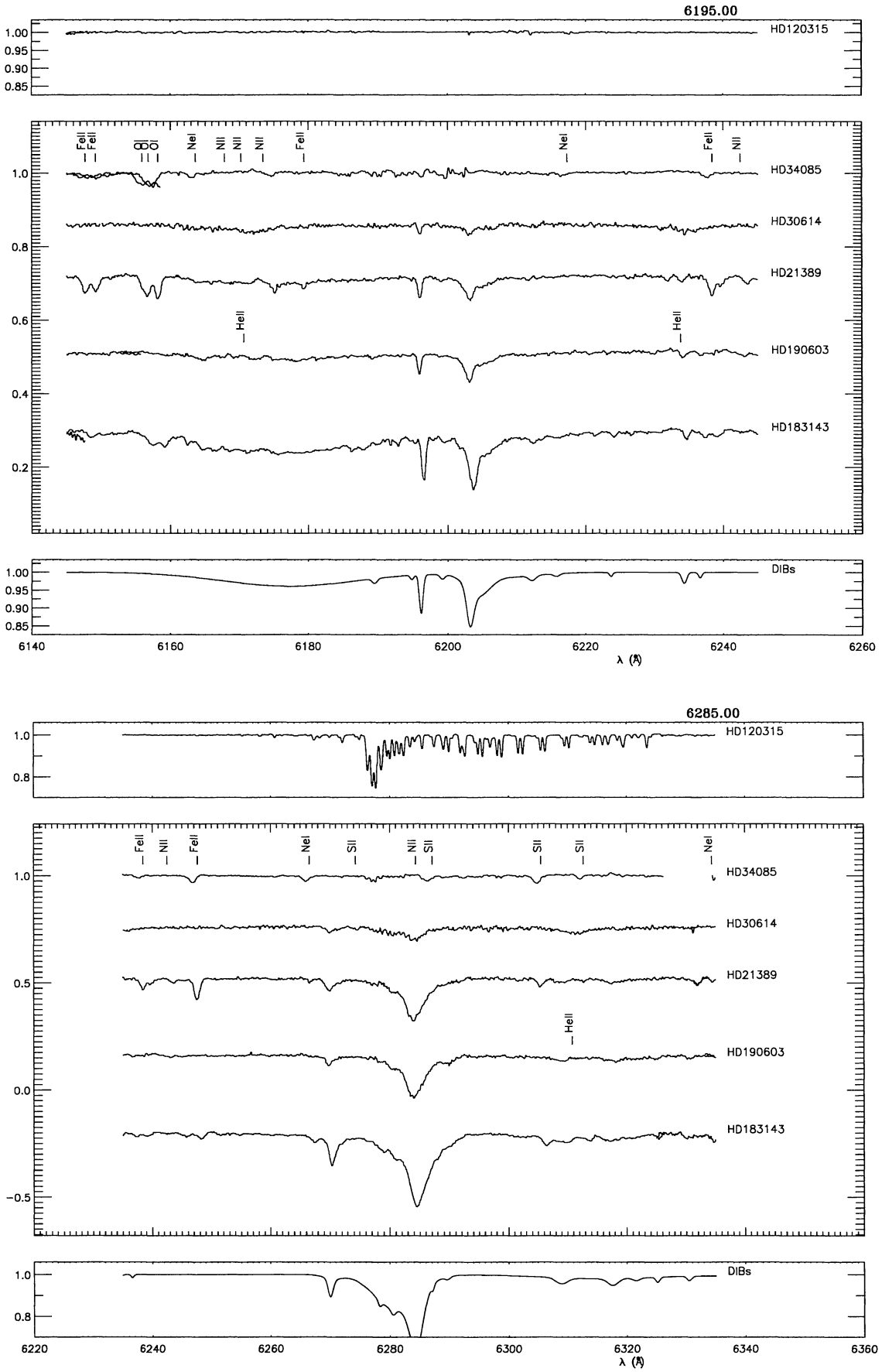

Fig. 6. continued

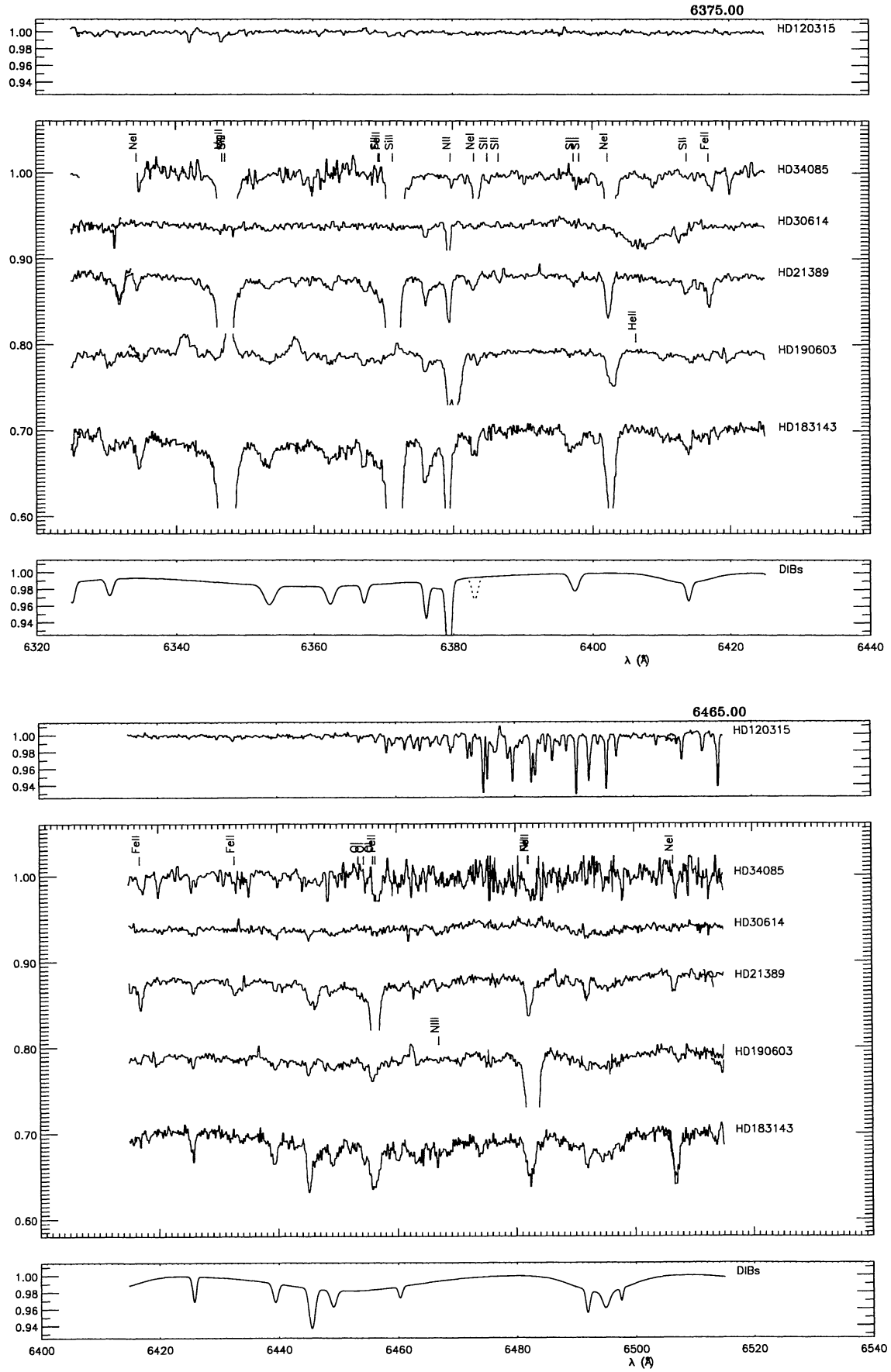

Fig. 6. continued

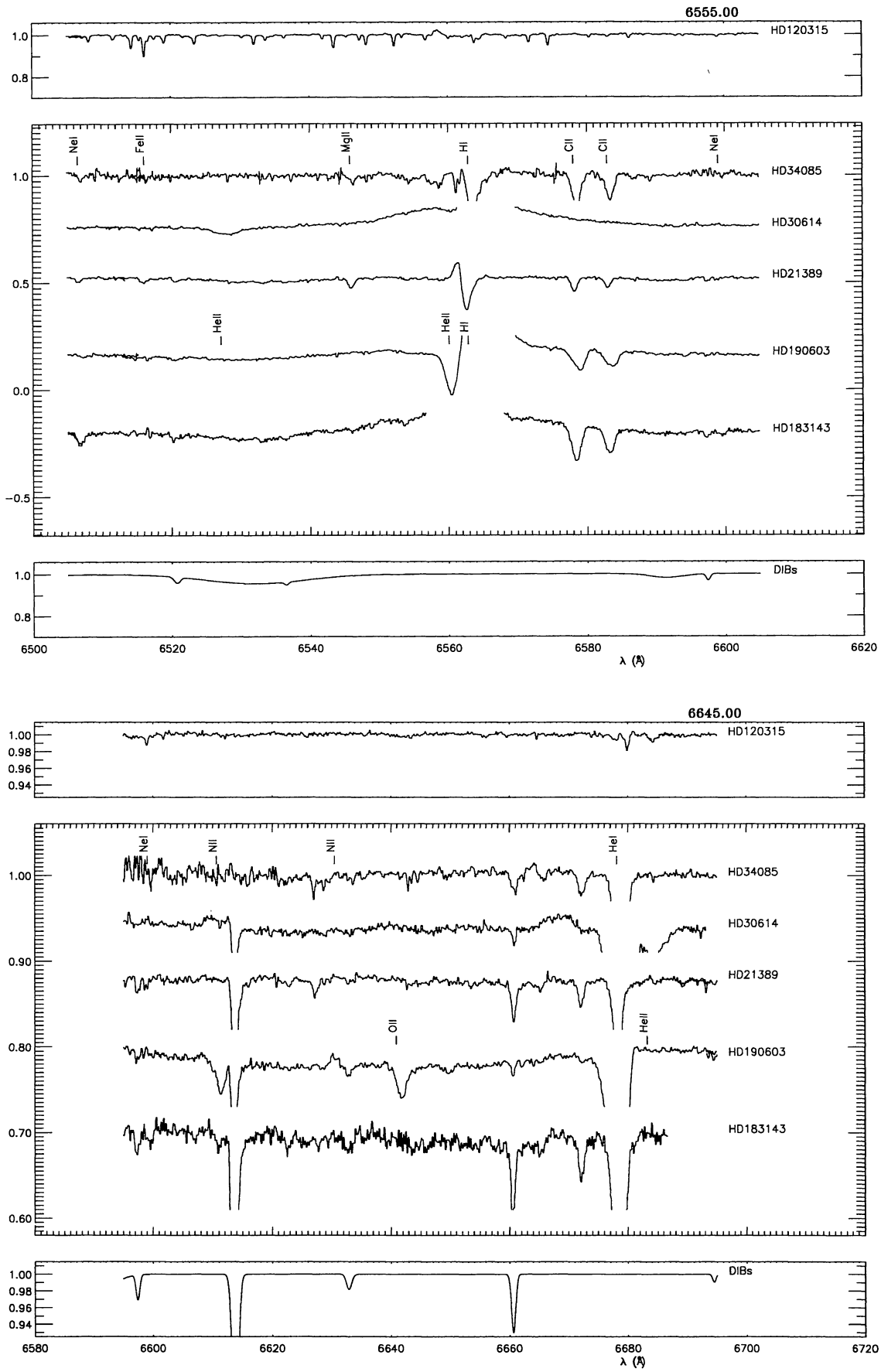

Fig. 6. continued

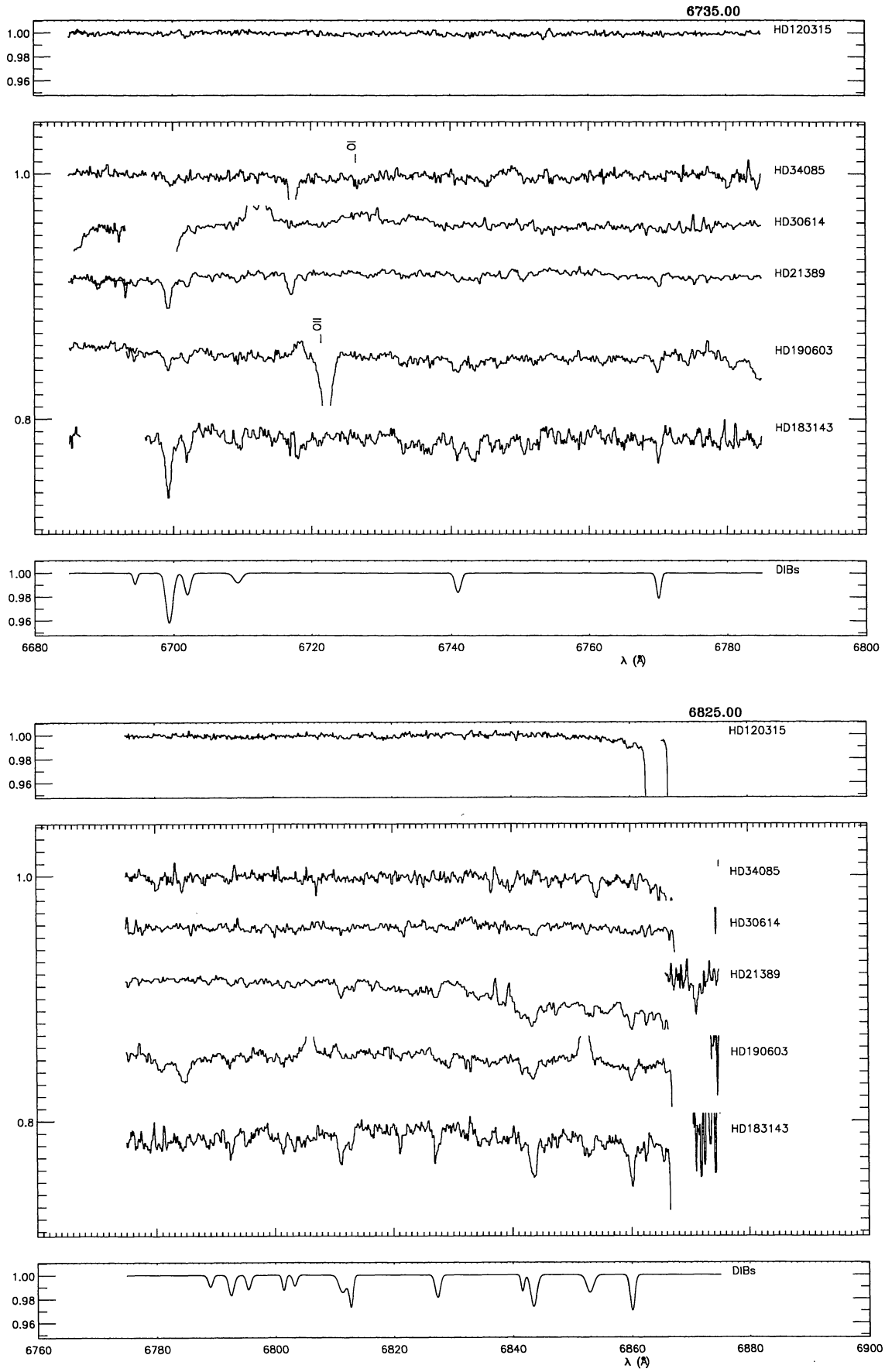

Fig. 6. continued

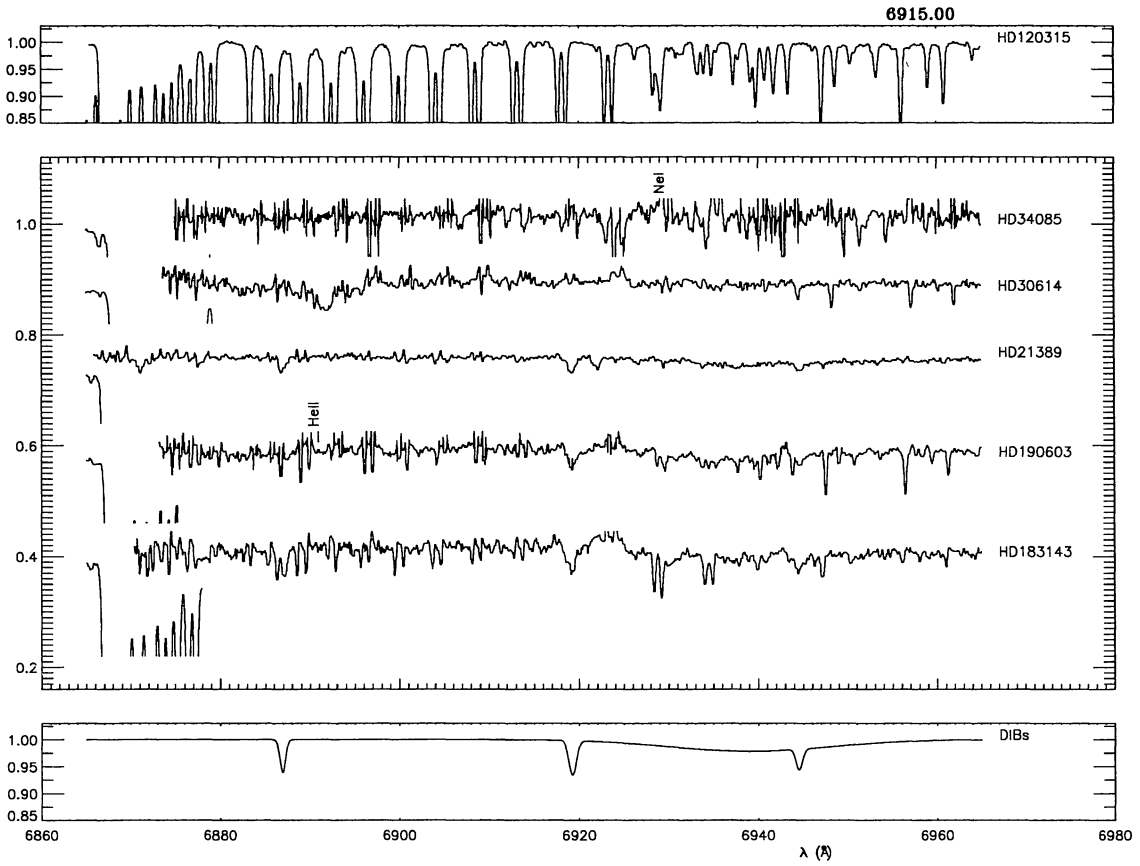

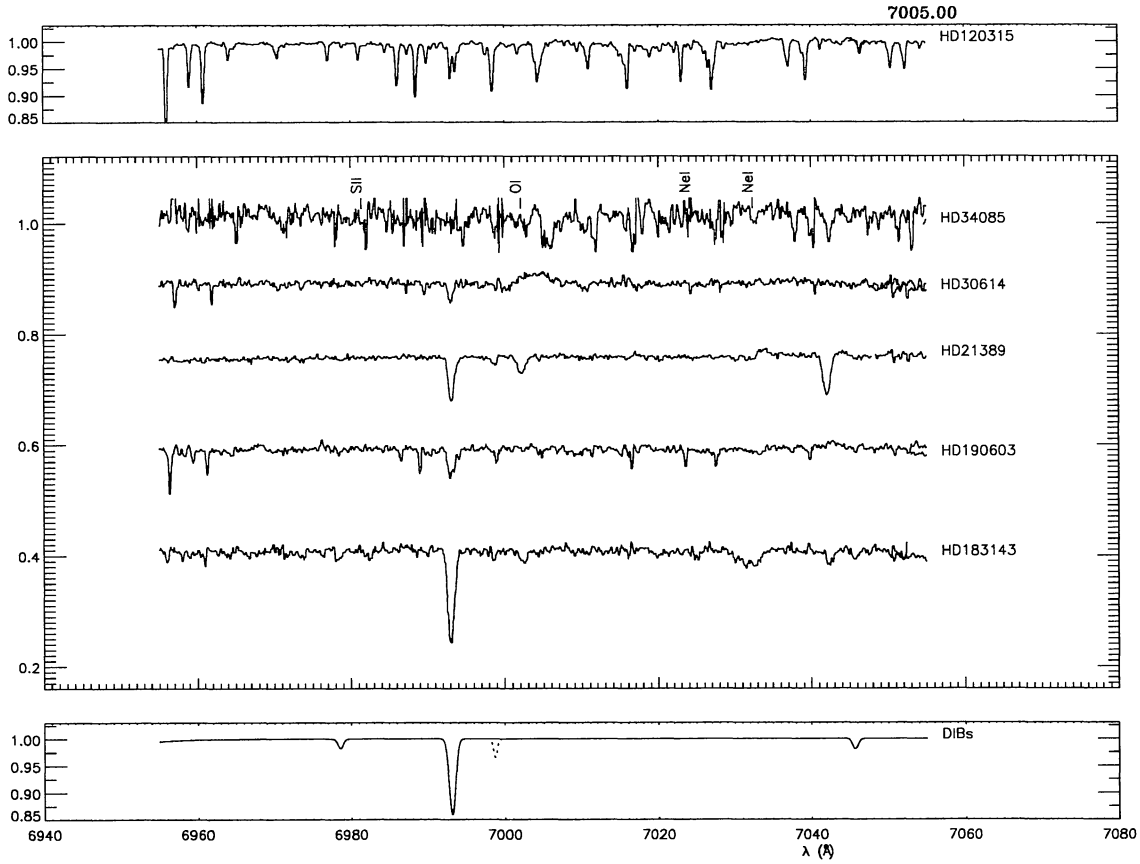

Fig. 6. continued

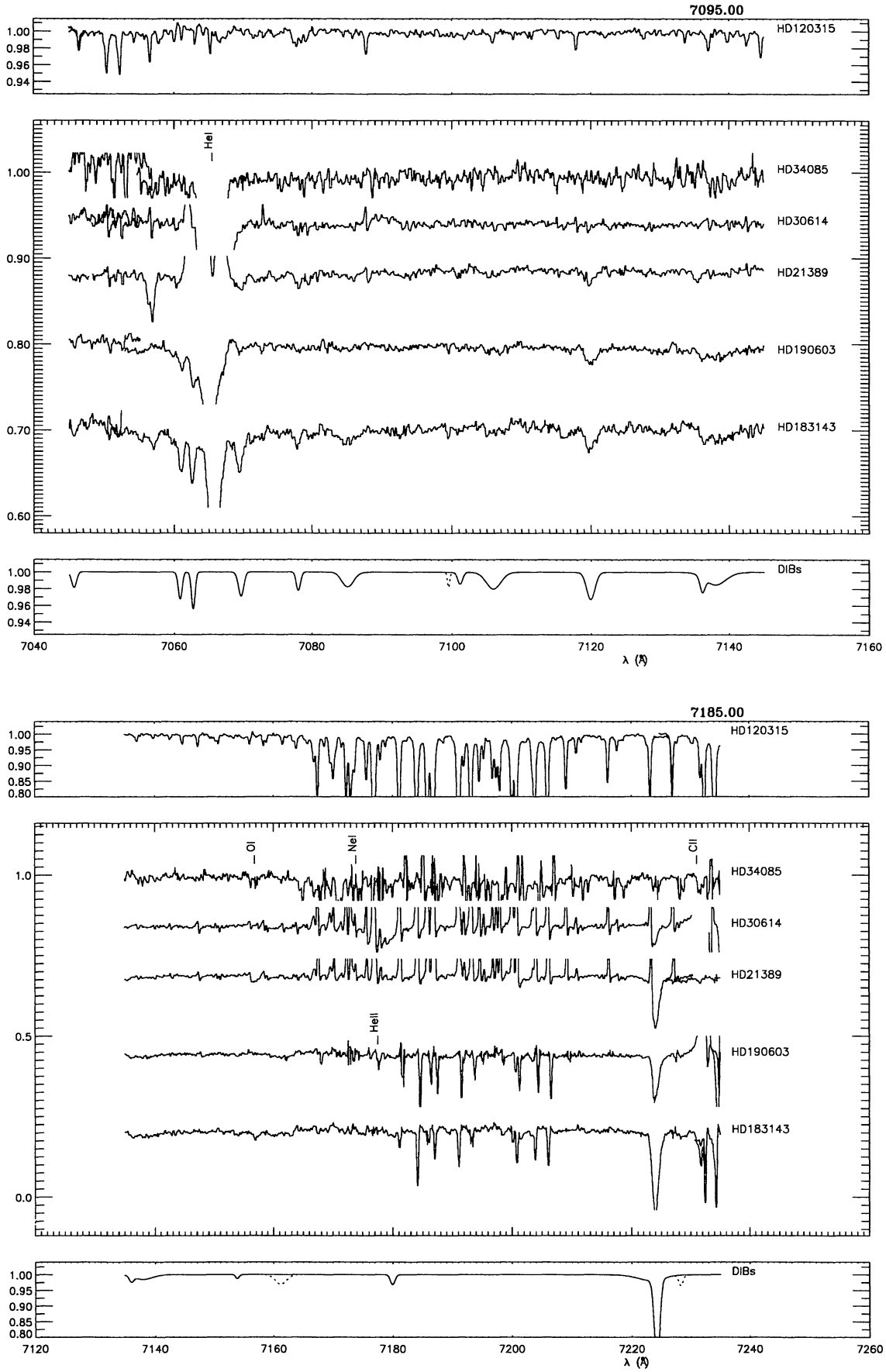

Fig. 6. continued

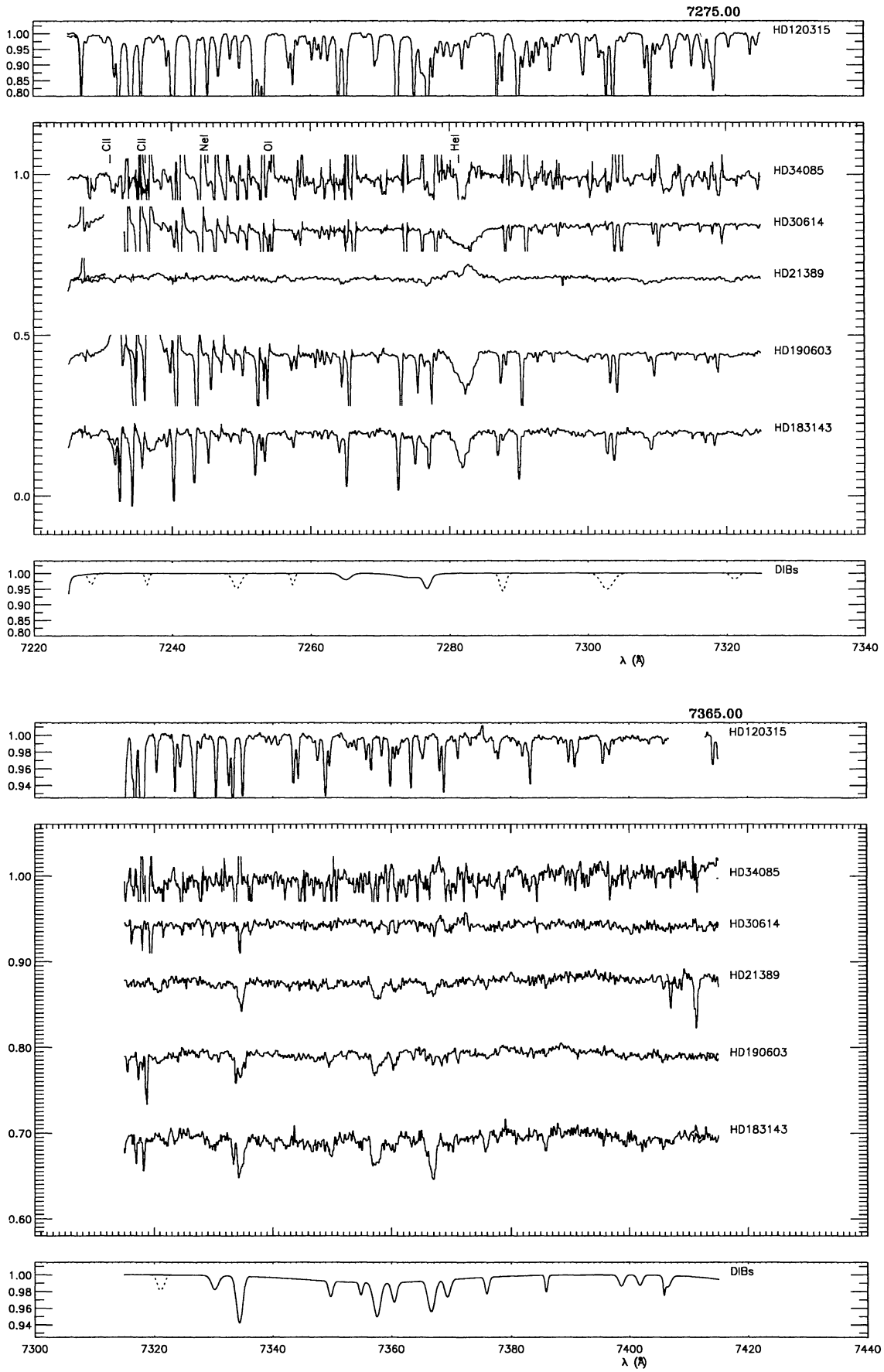

Fig. 6. continued

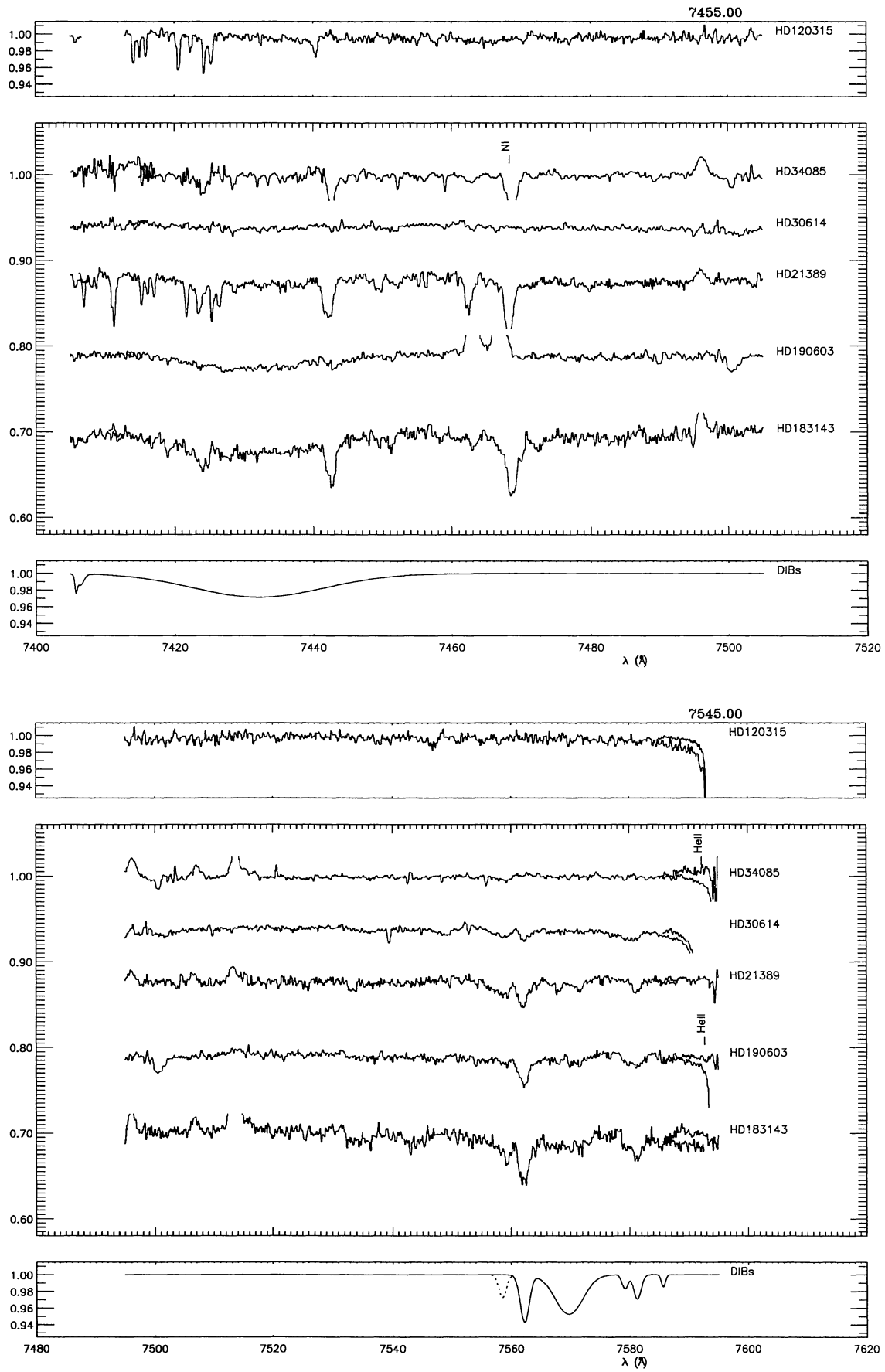

Fig. 6. continued

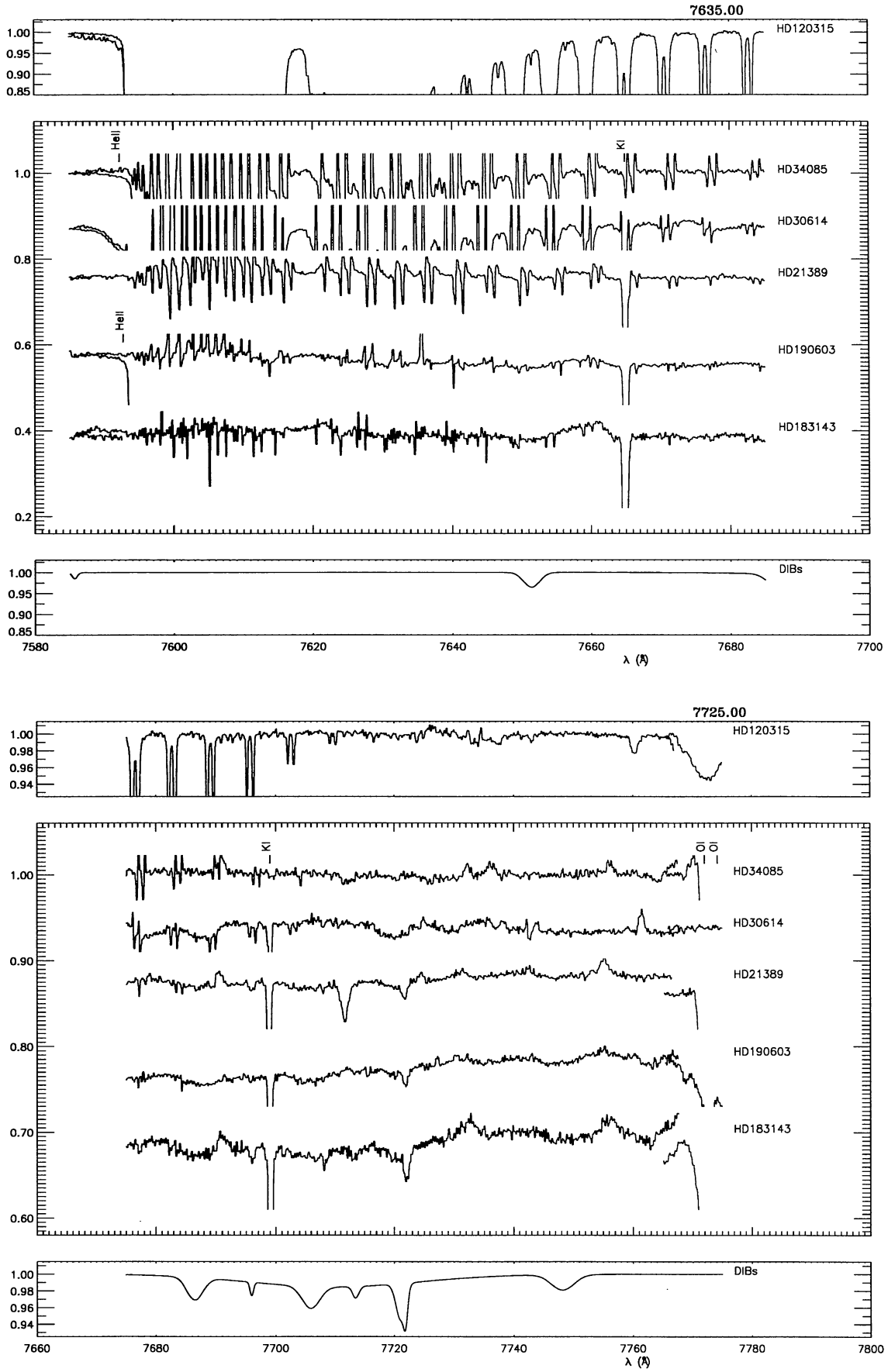

Fig. 6. continued

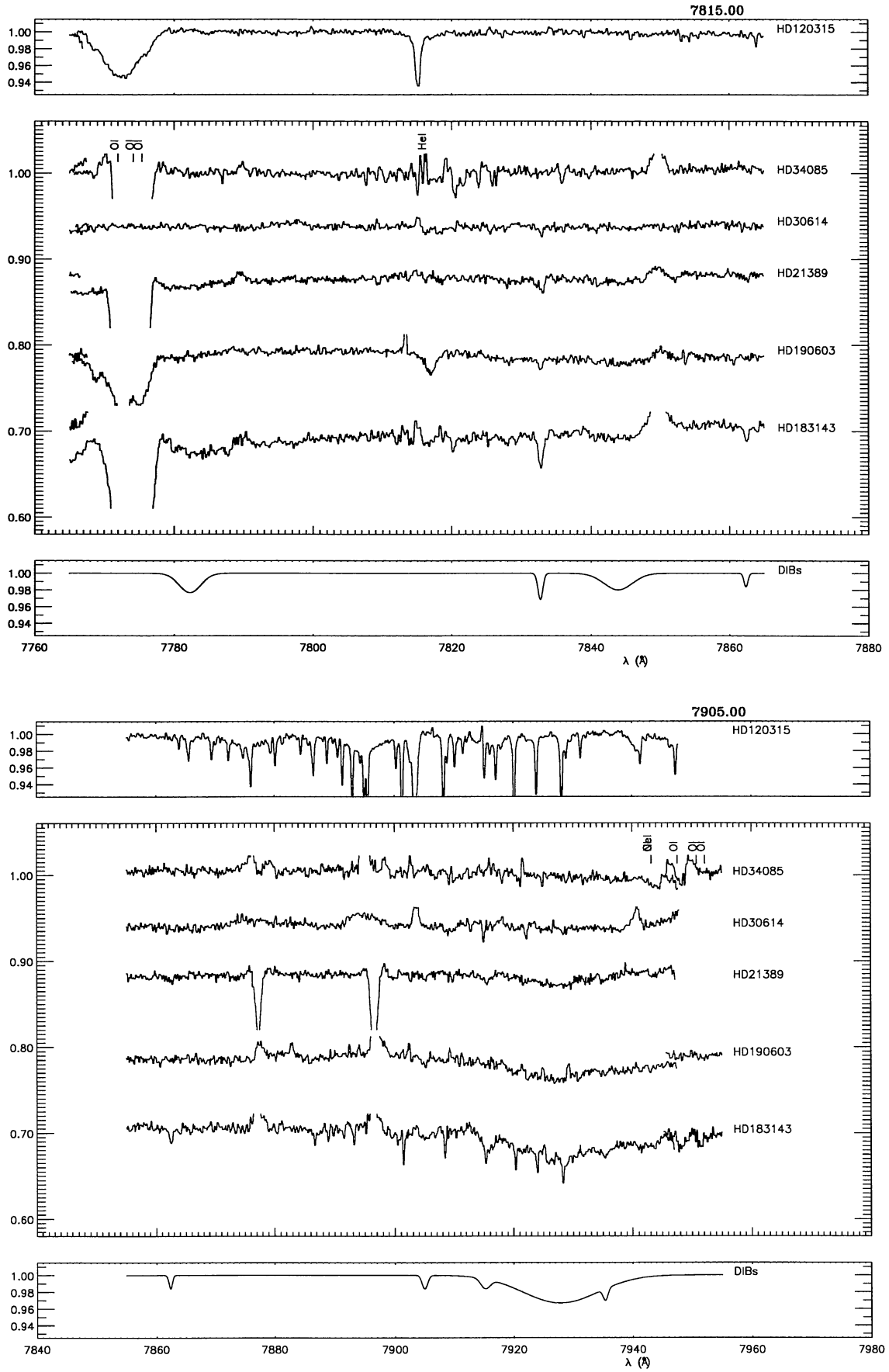

Fig. 6. continued

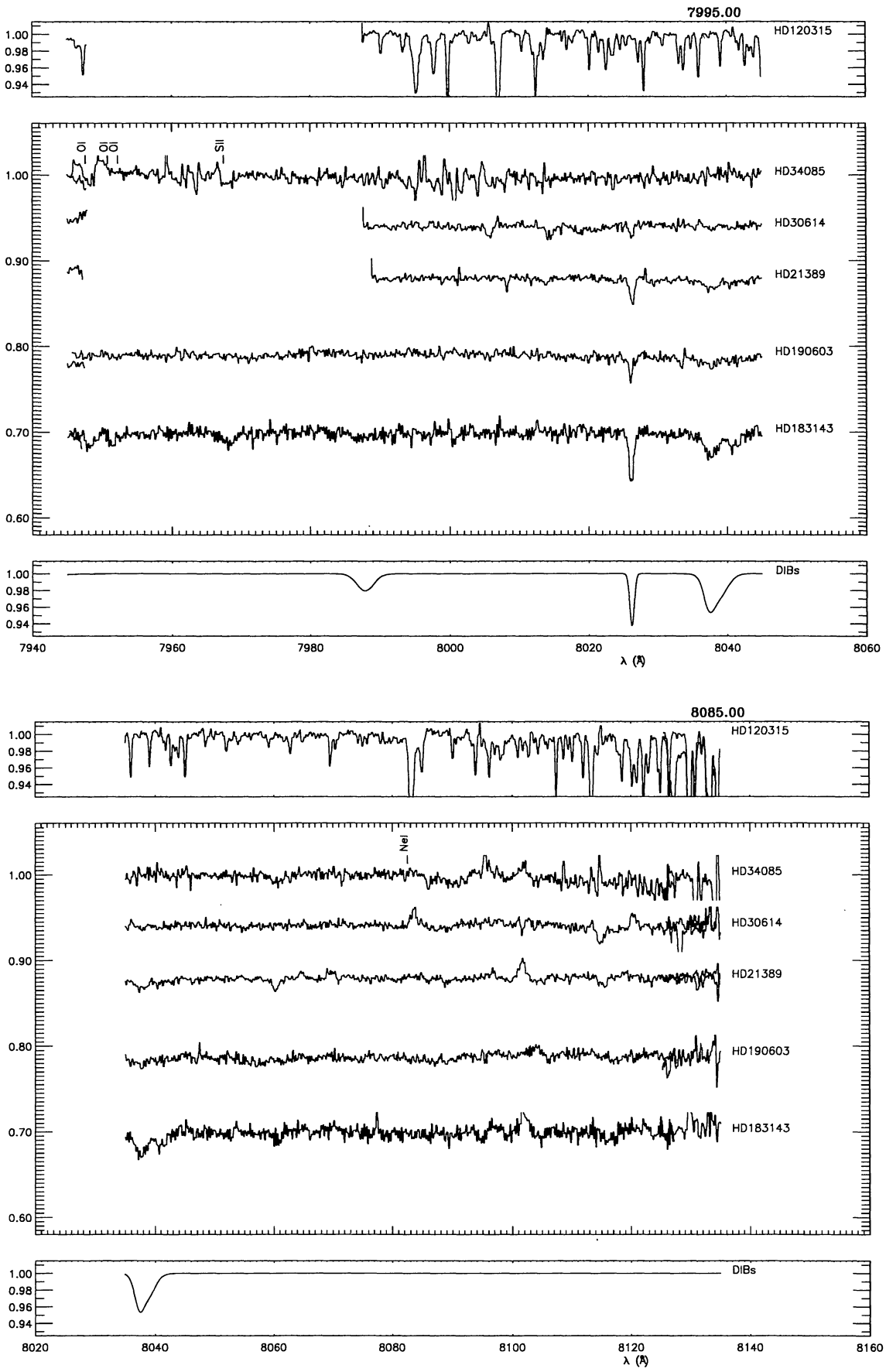

Fig. 6. continued

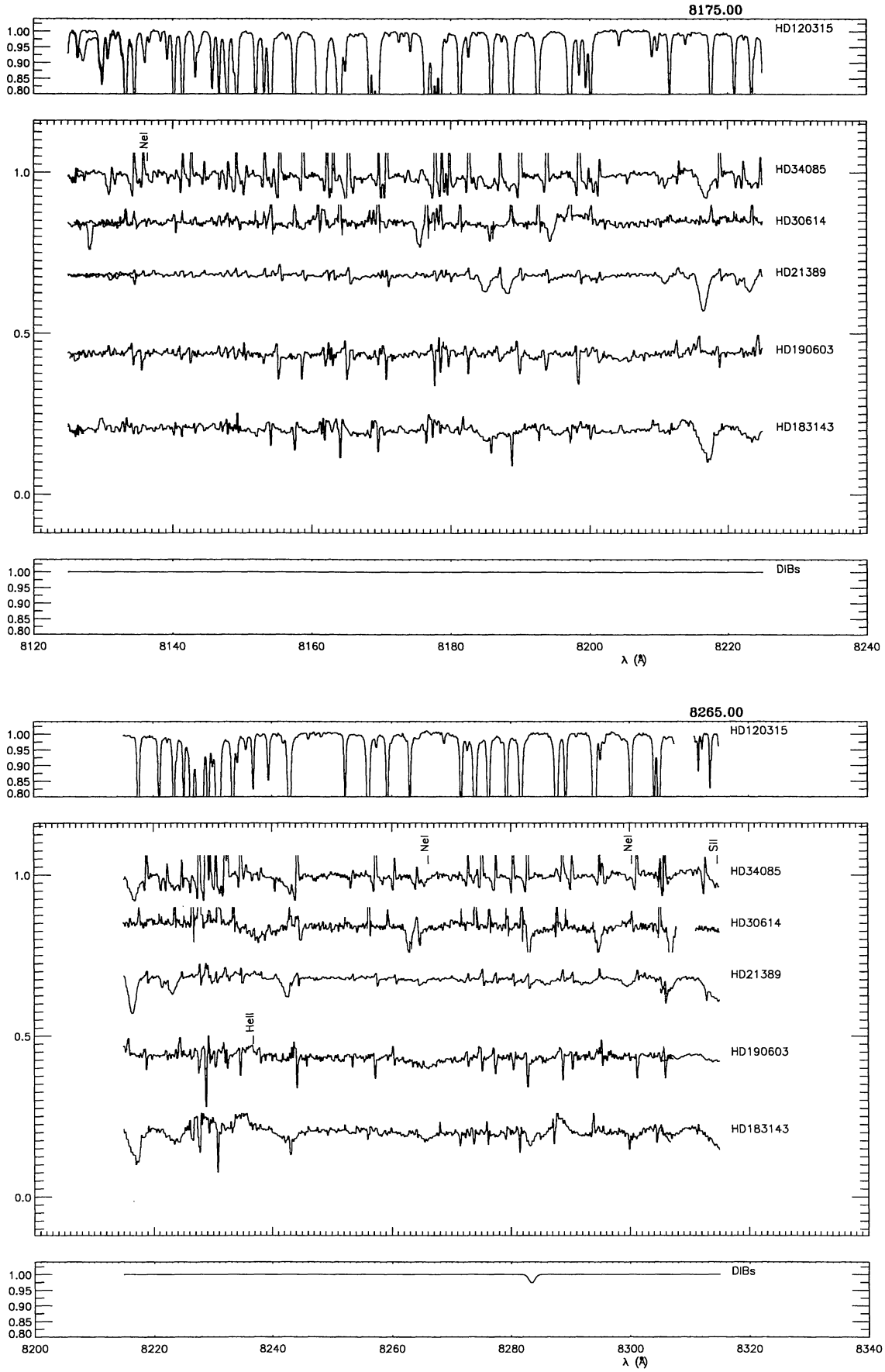

Fig. 6. continued

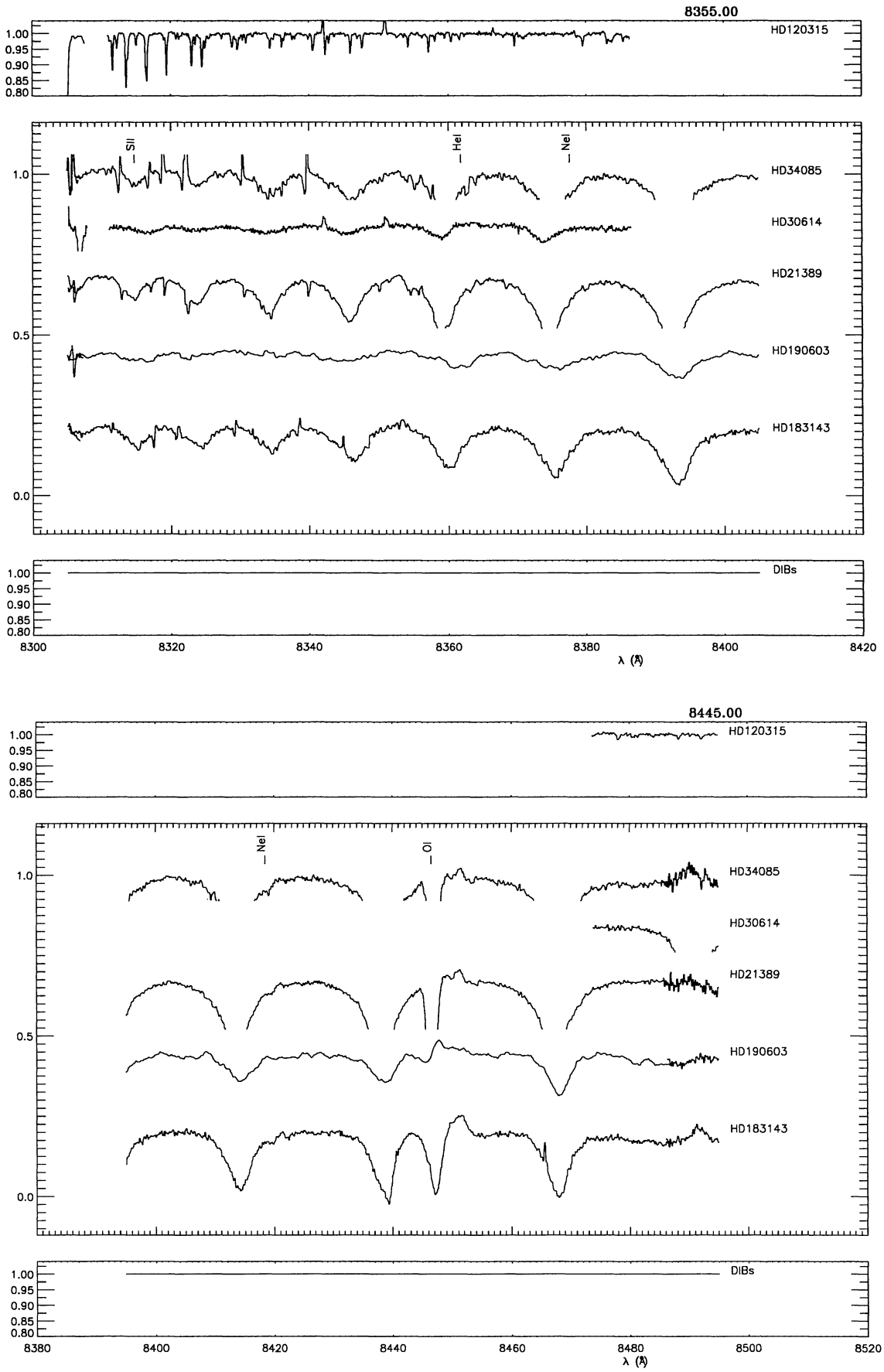

Fig. 6. continued

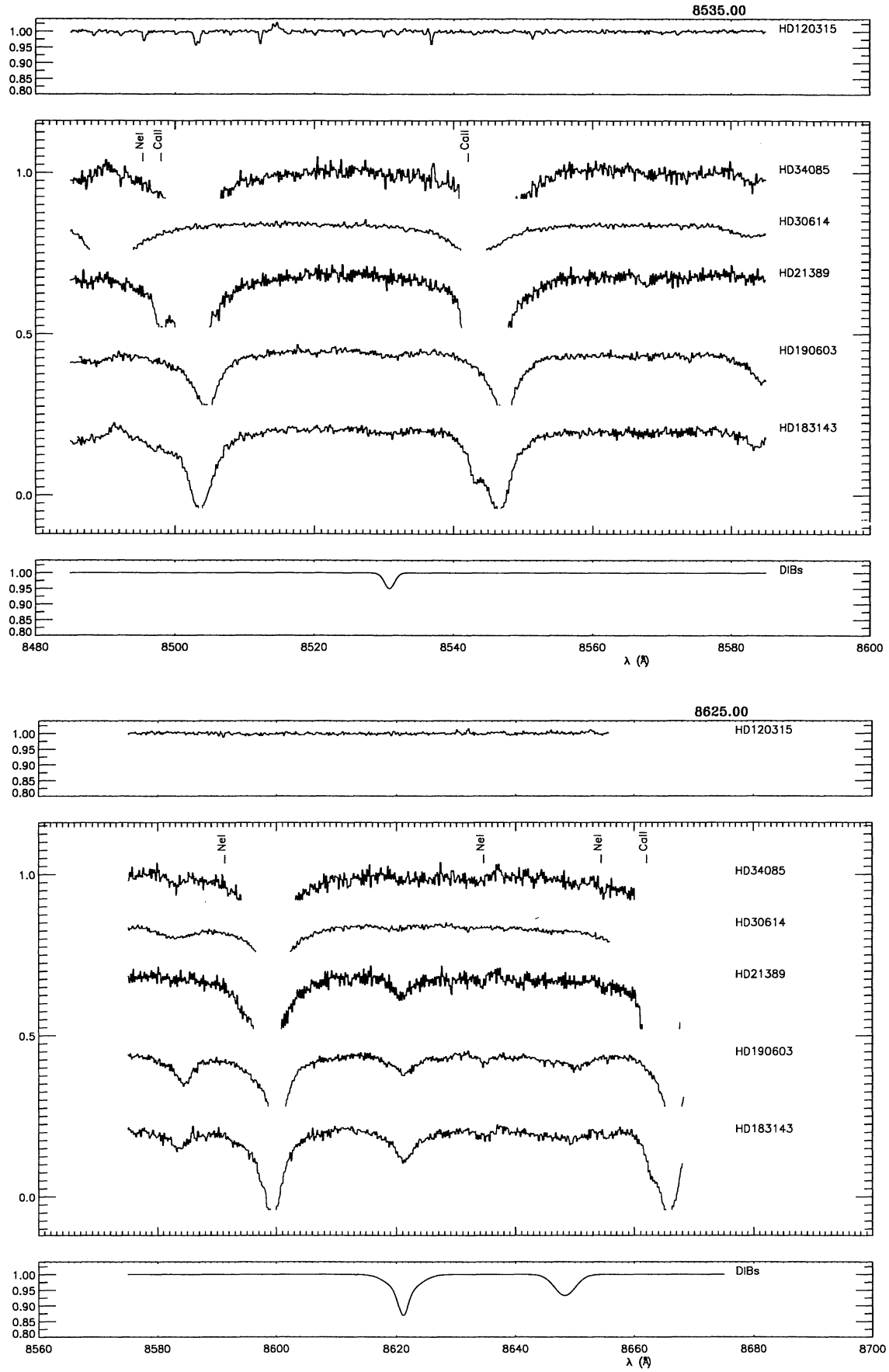

Fig. 6. continued